ACS OMEGA

Article

Influence of Aromatic Cations on the Structural Arrangement of Hg(II) Halides

Francisco Sánchez-Férez, Xavier Solans-Monfort, Teresa Calvet, Mercè Font-Bardia, and Josefina Pons*

Cite This: *ACS Omega* 2020, 5, 29357−29372

Read Online

ACCESS | Metrics & More | Article Recommendations | SI Supporting Information

ABSTRACT: Understanding the structure and arrangement of hybrid metal halides and their contribution to the optoelectronic properties is, thus far, a challenging topic. In particular, new materials composed of d^{10} metal halides and pyridinium cations are still largely unexplored. Therefore, we report the synthesis and characterization of six Hg(II) salts built up from $(Hg_2Cl_6)^{2-}$ or $(HgX_4)^{2-}$ anions (X = Cl, Br, I) and 2,2′-bipyridium (2,2′-Hbipy)$^+$, 2,2′-bipyridine-1,1′-diium (2,2′-H$_2$bipy)$^{2+}$, or 1,10-phenantrolinium (1,10-Hphen)$^+$ cations, using the same experimental conditions. All of them have been characterized by PXRD, EA, FTIR-ATR, and ^{1}H NMR spectroscopies; single-crystal X-ray diffraction; and TG/DTA determinations. The study of their packing via Hirshfeld surface analysis and 3D deformation density mapping revealed the contributions of the intermolecular interactions to the structural arrangement, notably, the effect of the cation planarity on them. Successively, periodic DFT calculations showed that (i) the valence and conducting bands are mainly composed of the p orbitals of the halide and the organic cation, respectively, and (ii) the corresponding band gap depends mainly on the halide.
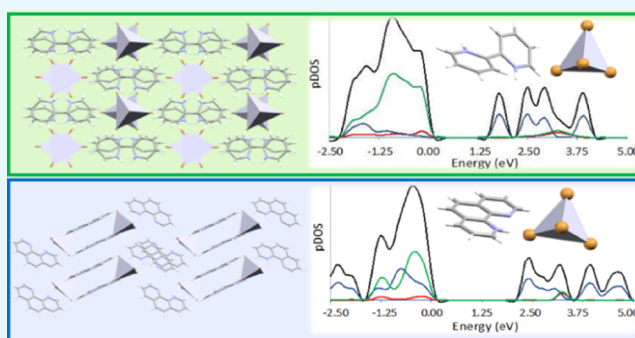
INTRODUCTION

The study of hybrid organic–inorganic materials composed of metal halide anions and ammonium-based organic cations has suffered a rekindled interest flagged by their application in optoelectronic devices. Their solvent processability and easy fabrication in combination with their structural tunability distinguished them as promising materials.[1,2]

As their structural arrangement directly affects the electronic properties, thoroughgoing studies on the effects of anion and cation into the final packing and their influence on the band gap are required. Indeed, the structural features of the cation (size, planarity, and aromaticity) conjointly with those of the anion (size, geometrical metal preferences, and halide dimensions)[3] are known to drive the assembly of the inorganic units through their intermolecular interactions (electrostatic, π···π stacking, anion···π, and σ-hole effects).[4–9]

Notwithstanding the extensive research done with primary amines and in a lesser extent with aromatic rings,[10] the studies incorporating pyridinium cations are scarce.[2,11] Howbeit, aromatic cations were proven to be remarkable candidates for preparing light-emitting compounds.[12] While alkyl ammonium cations tend to form layered arrays,[13,14] even more pronounced with large cations,[15] their replacement with bipyridinium rings with a delocalized π-electron character may, at the same time, modify the packing and the electronic properties.

Within this frame, there has been extensive research on Sn(II), Pb(II), and Ge(II) halides but less on Zn(II), Cd(II),

and Hg(II)[16–21] being prospective homovalent candidates. In previous papers, Hg(II) halides containing alkylammonium cations *inter alia*, $(C_3H_{12}N_2)(HgCl_4)$[22] and $(C_4H_{14}N_2)(HgCl_4)$,[23] presented corner-sharing HgCl$_6$ octahedra with $(HgCl_4)^{2-}$ units forming layers separated by the bifunctional ammonium cations. The larger aliphatic chain of $(C_4H_{14}N_2)^{2+}$ favored van der Waals interactions, better stacking the cations and favoring the shorter separation of the inorganic layers. Their substitution by benzidinium cations in $(NH_3(C_6H_4)_2NH_3)(HgCl_4)$[24] modified the inorganic connectivity, constructing tetrahedral HgCl$_4$ units but preserving the layered structure. In this case study, the aromatic benzidinium cations did not form π···π stacking interactions, which favored the separation of the inorganic units.

In addition, their spherical d^{10} closed-shell electronic configuration stands out for promoting the electronic transitions to occur through ligand-centered (LC) and ligand-to-ligand charge transfer (LLCT) and hence excels at presenting photophysical properties.[25] In this sense, to the best of our knowledge, there is no previously reported study on the

optoelectronic properties of Hg(II) halides incorporating pyridinium cations.

Our group has previously explored the structural behavior of d^{10} metal ions in the presence of either carboxylic aromatic ligands or combined with N-donor aromatic ligands, relating it with their photophysical properties.[26−28] In this contribution, we focused on Hg(II) halides in the presence of N-donor aromatic conjugated cations being 2,2′-bipyridium (2,2′-Hbipy)⁺, 2,2′-bipyridine-1,1′-diium (2,2′-H₂bipy)²⁺, and 1,10-phenantrolinium (1,10-Hphen)⁺, bearing on their different planarity and bulkiness. Herein, the synthesis of six hybrid Hg(II) halides, (2,2′-Hbipy)₂(Hg₂Cl₆) (**1**), (2,2′-H₂bipy)-(HgX₄) (X = Br (**2**), I (**3**)), and (1,10-Hphen)₂(HgX₄) (X = Cl (**4**), Br (**5**), and I (**6**)), is reported, and their single-crystal X-ray structures are determined. The study of their arrangements conjointly with periodic DFT calculations has enabled us to obtain more insight on the effect of these relatively unexplored cations with their corresponding halogen atom on the final packing and optoelectronic properties.

■ RESULTS AND DISCUSSION

Synthesis and General Characterization. All the reactions have been carried out by mixing HgX₂ (X = Cl, Br, I) with 2,2′-bipyridine (2,2′-bipy) or 1,10-phenantroline (1,10-phen) in a 1:2 molar ratio and acidified media with the corresponding acid (HCl, HBr, and HI) in a CH₂Cl₂/MeOH solvent mixture at room temperature (r.t.). The CH₂Cl₂/MeOH solvent mixtures were 2:1 (**1**, **2**, **4**, **5**) or 1:1 (**3**, **6**), relying on the low solubility of HgI₂ in CH₂Cl₂ (Scheme 1).

Scheme 1. Outline of the Synthesis of Compounds 1−6
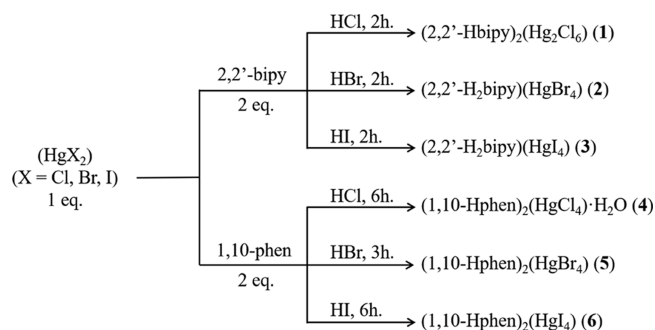
The formation of 2,2′-bipyridium (2,2′-Hbipy)⁺, 2,2′-bipyridine-1,1′-diium (2,2′-H₂bipy)²⁺, or 1,10-phenantrolinium (1,10-Hphen)⁺ cationic species resulted in compounds (2,2′-Hbipy)₂(Hg₂Cl₆) (**1**), (2,2′-H₂bipy)(HgX₄) (X = Br (**2**) and I(**3**)), and (1,10-Hphen)₂(HgX₄) (X = Cl (**4**), Br (**5**), and I (**6**)). All these compounds have been characterized by PXRD, EA, FTIR-ATR, and ¹H NMR spectroscopies; single-crystal X-ray diffraction; and TG/DTA determination. It should be mentioned that even if the crystal structure of **2** was previously reported by Ali and Al-Far,[29] it was determined at 297 K rather than at 100 K, which leads to slight changes in the unit cell and intermolecular interactions. In addition, the synthesis was performed using a different synthetic method.

Phase purity of the bulk samples was confirmed by PXRD (Supporting Information, Figure S1). In the FTIR-ATR spectra of **1−6**, the $v(N-H^+)$ appeared as a broad band between 3448 and 2712 cm⁻¹ and probably shifted to a minor wavenumber due to the strong ionic interaction between the proton and the corresponding halogen atom.[30] This is reflected

in the spectrum of compound **6** in which the N−H⁺ group is not hydrogen bonded to the (HgI₄)²⁻ anion and thus, the $v(N-H^+)$ peak is shifted to higher values. In addition, the formation of C−H···X interactions provoked a redshift on the $v_{ar}(C-H)$ modes of the cations. Since the strength of these associations depend on the electronegativity of the acceptor,[31] the shift is in line with the order Cl > Br > I, ranging from 3094 to 3022 cm⁻¹. The bands attributable to $v(C=C/C=N)$ and $\delta(N-H^+)$ appeared in the region between 1635 and 1443 cm⁻¹, while $\delta(C=C/C=N)$ ring modes[32] appeared between 1428 and 1370 cm⁻¹. The aromatic C−H vibrational modes of the cations are also identified between 1185 and 1165 cm⁻¹ $[\delta(C-H)_{ip}]$ or between 844 and 714 cm⁻¹ $[\delta(C-H)_{oop}]$[33] (Supporting Information, Figures S3−S8). An additional band from the $\gamma(N-H)^+$ out-of-plane mode[30] is identified from 960 to 917 cm⁻¹.

The ¹H NMR spectra of **1−6** have been recorded in DMSO-d_6 solution. They show four signals between 8.90 and 7.81 ppm (**1−3**) or between 9.32 and 8.18 ppm (**4−6**) assigned to the aromatic protons of the cations, which are shifted with respect to the free 2,2′-bipy and 1,10-phen molecules (8.68−7.44 ppm and 9.10−7.76 ppm, respectively), indicating a change of the electronic distribution caused by the protonation of the corresponding N-donor atoms. The N−H⁺ protons appear from 5.32−4.73 ppm in **1−3** and between 4.10−4.39 ppm in **4−6**.[34] Further NMR details are provided in the Experimental Section (Supporting Information, Figures S9−S14).

Finally, the TG/DTA determination of the samples enabled to analyze their thermal stability showing that they are stable until at least 220 °C (Supporting Information, Figure S15).

Crystal and Extended Structure of (2,2′-Hbipy)₂(Hg₂Cl₆) (1). Compound **1** is composed of a dimeric (Hg₂Cl₆)²⁻ anion and two (2,2′-Hbipy)⁺ cations in cis conformation. The (Hg₂Cl₆)²⁻ unit is formed around two Hg(II) centers at 3.8978 (4) Å (slightly longer than other reported Hg···Hg distances, 3.7523 (3)−3.884 (4) Å), displaying a distorted tetrahedral geometry (τ_4(Hg (1)) = 0.80; τ_4(Hg (2)) = 0.72)[35] and being connected through two asymmetrically bridging Cl and four terminal Cl atoms (Figure 1a). All the Hg−Cl bond lengths fall within the range 2.3745 (9)−2.8758 (8) Å (Table 1), which are in accord with reported (Hg₂Cl₆)²⁻ containing compounds (2.370 (2)−2.881 (2) Å).[36−39]

These dimeric units are held together in a linear fashion through the *a* axis by interdimeric interactions between the Hg(II) centers and the terminal Cl (Hg (2)···Cl (1), 3.1429 (7) Å and Hg (1)···Cl (5), 3.3911 (8) Å) (being 3.30 Å the sum of the van der Waals radii of both atoms). The 2,2′-Hbipy cations are disposed around these chains, being N−H oriented to the remaining terminal Cl via hydrogen bond interactions. At both sides and parallel to the (Hg₂Cl₆)²⁻ chain, the 2,2′-Hbipy cations are stacked through π···π interactions (Figure 1b) in an alternate manner (double-single and so forth): double (pyridyl−pyridyl and pyridinium−pyridinium) and single (pyridyl−pyridyl) (Table 1). These 2,2′-Hbipy cations associate the chains forming a 3D net.

Crystal and Extended Structure of (2,2′-H₂bipy)-(HgBr₄) (2). Compound **2** was previously reported[29] by Ali and Al-Far,[29] but we extended the structural study considering further interactions relevant for this paper. It is composed of one monomeric (HgBr₄)²⁻ anion and two (2,2′-H₂bipy)²⁺ cations (Figure 2a), in which the Hg(II) center displays a
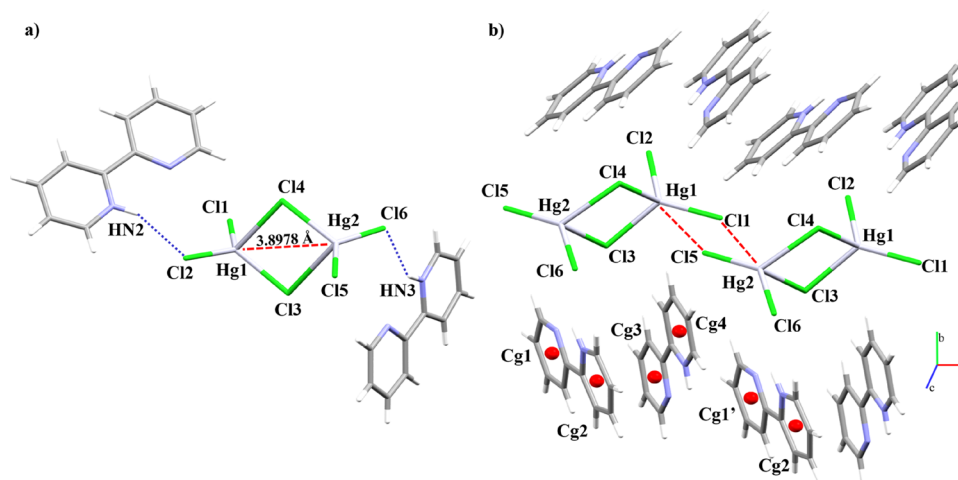
Figure 1. (a) Molecular structure of $(2,2\text{'-Hbipy})_2(Hg_2Cl_6)$ (**1**) highlighting the ionic interactions between the 2,2'-Hbipy cations and the chlorine atoms. (b) 1D expansions of the dimeric units through Hg⋯Cl and $\pi\cdots\pi$ interactions.

slightly distorted tetrahedral geometry $(\tau_4(Hg\ (1)) = 0.86)$.[35] These anions are joined through ionic interactions into 1D chains along the *a* axis via bridging *trans*$(2,2\text{'-H}_2\text{bipy})^{2+}$ (Figure 2b). It should be noted that there is an interaction between the Br (3) atom and the subsequent Hg(II) center of a contiguous monomeric unit at 3.5785 (5) Å (longer than the sum of their van der Waals radii: 3.40 Å).

Even though it could not be considered a coordination bond, it is a non-negligible interaction since it directs the $(HgBr_4)^{2-}$ stacking through the *c* axis and lengthens the Hg (1)−Br (3) bond (2.7985 (5) Å) compared to the rest (2.5491 (4)−2.6299 (4) Å). All the Hg−Br bond lengths are similar to the previously reported structure[29] and within the range of other reported compounds with $(HgBr_4)^{2-}$ anions and pyridinium cations[12] (2.6328 (4)−2.6900 (5) Å) (Table 2). In this case, the 2,2'-H_2bipy rings are too far to assemble by $\pi\cdots\pi$ interactions (4.774 Å) (Figure 2b).

Finally, the 2,2'-H_2bipy cations interact both supporting the stacking of the inorganic units via C−H⋯Br interactions (C (4)−H (4)⋯Br (3), 2.9257 Å; C (7)− H (7)⋯Br (1), 2.8372 Å; C (1)−H (1)⋯Br (4), 2.7677 Å; and C (12)−H (12)⋯Br (4), 2.8960 Å) and joining the chains through N−H⋯Br ionic associations (N (1)−H (1N)⋯Br (3), 2.3852 Å and N (2)−H (2N)⋯Br (2), 2.4593 Å), which form a 2D layer along the *ac* plane (Figure 2c) (Table 2).

Crystal and Extended Structure of $(2,2\text{'-H}_2\text{bipy})(HgI_4)$ (3). Compound **3** is composed of a monomeric $(HgI_4)^{2-}$ anion and two $(2,2\text{'-H}_2\text{bipy})^{2+}$ cations. The Hg(II) center has a tetrahedral geometry $(\tau_4(Hg\ (1)) = 0.94)$[35] (Figure 3a) (Table 3). These anions are discrete units without any significant interactions between them and surrounded by $(2,2\text{'-H}_2\text{bipy})^{2+}$ cations through N−H⋯I ionic associations (N (1)−H (1N)⋯I (2), 2.6524 Å and N (2)−H (2N)⋯I (1), 2.5764 Å) and weak C−H⋯I interactions, which form linear zigzag chains along the *b* axis (Figure 3b) (Table 3). The Hg−I bond lengths (2.7398 (5)−2.8398 (5) Å) are within the range of reported $(HgI_4)^{2-}$ anions (2.7430 (8)−2.844 (1) Å).[40−42]

Only weak reciprocal C−H⋯I contacts join the chains along the *c* axis (C (8)−H (8)⋯I (4), 3.1363 Å and H (8)−C (8)⋯I (4), 3.895 (7) Å; 138.10°), defining 2D layers through the *bc* plane and as in the case of **2**, $(2,2\text{'-H}_2\text{bipy})^{2+}$ cations are too far to be stacked trough $\pi\cdots\pi$ interactions (4.360 Å).

Crystal and Extended Structure of $(1,10\text{-}$Hphen$)_2(HgX_4)$ (X = Cl (4), Br (5), or I (6)). Compounds **4−6** are composed of $(HgX_4)^{2-}$ (X = Cl (**4**), Br (**5**), or I (**6**)) anions and 1,10-Hphen cations mainly associated through N−H⋯X, N−H⋯O, and C−H⋯X interactions (Figure 4). In the three compounds, the monomeric Hg(II) centers display a slightly distorted tetrahedral geometry (**4**: $\tau_4(Hg\ (1)) = 0.92$; **5**: $\tau_4(Hg\ (1)) = 0.91$; **6**: $\tau_4(Hg\ (1)) = 0.95$).[35] The Hg−X bond lengths are within the range of reported $(HgX_4)^{2-}$ anions[12,36−42] (Table 4).

In **4**, each Hg(II) node interacts with two $(1,10\text{-Hphen})^+$ cations either directly N (2)−H(2N)⋯Cl (2) (2.4169 Å) or through a water molecule N (4)−H(4N)⋯O (1.855 Å) and O(1 W)−H(1WB)⋯Cl (4) (2.375 (2) Å) (Table 5). This double association alters the intermolecular interactions, forming zigzag 1D chains along the *c* axis (Figure 5a).

In two previously reported closely related case studies, the mono- or diprotonated 1,10-phenantrolines in $(\text{phenH})_2[ZnCl_4]\cdot H_2O$ or $(\text{phenH}_2)_2Pb_3I_{10}\cdot 2H_2O$ also interact through water molecules rather than directly with the corresponding halogen atoms.[2,43] There are precedents demonstrating the strength of the Cl⋯H_2O interaction.[44] In addition, $(HgCl_4)^{2-}$ anions are surrounded by six $(1,10\text{-}$Hphen$)^+$ cations stacked in pairs by reciprocal $\pi\cdots\pi$ interactions (Figure 5b) and associated with the anion via combination of C−H⋯Cl and N−H⋯Cl. In addition, these cations are weakly interacting with neighboring anions by Cl⋯π[4,5] (Figure 5c) ,which form a 3D net.

In **5**, two $(1,10\text{-Hphen})^+$ cations associate with a $(HgBr_4)^{2-}$ anion through double N−H⋯Br and C−H⋯Br interactions within the range of similar compounds[12] (Table 6). In addition, these anions are surrounded by $(1,10\text{-Hphen})^+$ cations disposed in five pairs stacked by double (Figure 6a) or triple (Figure 6b) $\pi\cdots\pi$ interactions and a weak Br⋯π contact[4,5] (Figure 6c). These planar associations hold together the $(1,10\text{-Hphen})_2(HgBr_4)$ assemblies, forming a 3D net.

In **6**, the structural disorder limits the analysis of the intermolecular interactions; however, N atoms are too far from the I and thus, there is not any N−H⋯I interaction. Instead, the $(HgI_4)^{2-}$ anions associate through C−H⋯I interactions with eight $(1,10\text{-Hphen})^+$ cations (Figure 7a), which are stacked in chains by reciprocals pyridinium-phenyl $\pi\cdots\pi$ interactions (Table 7) along the *a* axis in a piled disposition
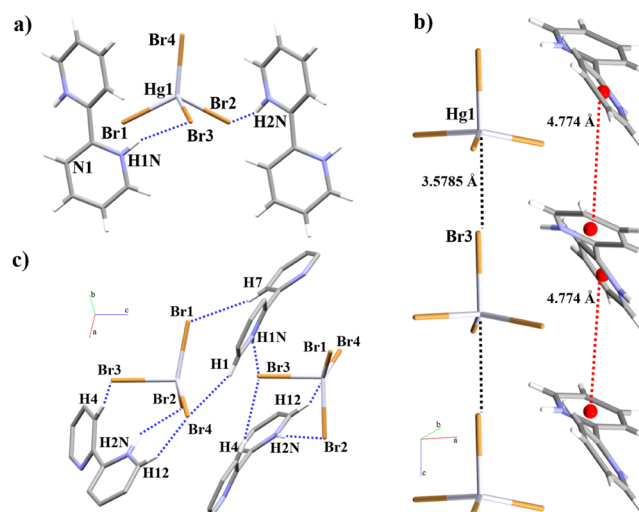
Table 1. Selected Bond Lengths, Angles, and Intermolecular Interactions of (2,2′-Hbipy)$_2$(Hg$_2$Cl$_6$) (1)^a

bond lengths (Å)			
Hg (1)–Cl (1)	2.4082 (8)	Hg (2)–Cl (6)	2.4092 (8)
Hg (1)–Cl (2)	2.4116 (7)	Hg (2)–Cl (4)	2.5527 (7)
Hg (1)–Cl (3)	2.5179 (8)	Hg (2)–Cl (3)	2.8757 (7)
Hg (1)–Cl (4)	2.7273 (7)	Hg (1)···Hg (2)	3.8978 (4)
Hg (2)–Cl (5)	2.3745 (8)		

bond angles (°)			
Cl (2)–Hg (1)–Cl (1)	127.81 (3)	Cl (5)–Hg (2)–Cl (4)	121.97 (3)
Cl (2)–Hg (1)–Cl (3)	108.80 (3)	Cl (6)–Hg (2)–Cl (4)	100.03 (3)
Cl (1)–Hg (1)–Cl (3)	120.05 (3)	Cl (5)–Hg (2)–Cl (3)	91.61 (3)
Cl (2)–Hg (1)–Cl (4)	103.99 (3)	Cl (6)–Hg (2)–Cl (3)	103.18 (2)
Cl (1)–Hg (1)–Cl (4)	95.24 (2)	Cl (4)–Hg (2)–Cl (3)	84.26 (2)
Cl (3)–Hg (1)–Cl (4)	88.08 (2)	Hg (1)–Cl (3)–Hg (2)	92.31 (2)
Cl (5)–Hg (2)–Cl (6)	136.77 (3)	Hg (2)–Cl (4)–Hg (1)	95.10 (2)

intermolecular interactions				
interaction	H···A (Å)	D···A (Å)	D–H (Å)	>D–H···A (°)
N (2)–H (2N)···Cl (2)	2.4434	3.250 (3)	0.880	152.68
N (3)–H (3N)···Cl (6)	2.4437	3.178 (3)	0.880	141.30
C (1)–H (1)···Cl (4)	2.8228	3.674 (3)	0.950	149.63
C (3)–H (3)···Cl (6)	2.9393	3.669 (3)	0.949	134.60
C (7)–H (7)···Cl (3)	2.5997	3.435 (3)	0.951	146.88
C (9)–H (9)···Cl (3)	2.8970	3.605 (5)	0.950	132.27
C (10)–H (10)···Cl (5)	2.8786	3.620 (4)	0.951	135.68
C (11)–H (11)···Cl (5)	2.8979	3.612 (3)	0.950	132.83
C (12)–H (12)···Cl (2)	2.8724	3.476 (3)	0.950	122.48
C (13)–H (13)···Cl (2)	2.9238	3.509 (3)	0.950	121.01
C (14)–H (14)···Cl (1)	2.9350	3.881 (3)	0.950	174.41

π···π interactions				
Cg (1)···Cg (3)	3.739 Å	69.71°	Cg (2)···Cg (4)	3.635 Å	71.68°
Cg (1)′···Cg (3)	3.653 Å	67.98°		

^{a}Cg (1) = Cg (1)′: N1–C1–C2–C3–C4–C5; Cg (2): N2–C6–C7–C8–C9–C10; Cg (3): N4–C16–C17–C18–C19–C20; Cg (4): N3–C11–C12–C13–C14–C15.

(Figure 7b). These chains are held together by the anions forming a 3D net.

Packing Analysis of 1−6. *General Considerations.* Some remarks should be examined to better comprehend these structural arrangements. We will emphasize the role of the halogen atoms (regarding their electronegativities, radii, and polarizabilities) and the organic units (planarity, mono- or diprotonation, and thus, their different electronic density distributions). Noteworthy is the increased role of weak

Figure 2. (a) Molecular structure of (2,2′-H$_2$bipy)(HgBr$_4$) (2) highlighting the ionic interactions between the 2,2′-H$_2$bipy cations and the bromine atoms. (b) Linear Br···Hg associations and (c) intermolecular interactions between (2,2′-H$_2$Bipy)$^{2+}$ and Br atoms.

Table 2. Selected Bond Lengths, Angles, and Intermolecular Interactions of (2,2′-H$_2$bipy)(HgBr$_4$) (2)

bond lengths (Å)			
Hg (1)–Br (1)	2.4082 (8)	Hg (1)–Br (4)	2.7273 (7)
Hg (1)–Br (2)	2.4116 (7)	Hg (1)···Br (3)	3.5785 (5)
Hg (1)–Br (3)	2.5179 (8)		

bond angles (°)			
Br (4)–Hg (1)–Br (1)	122.503 (11)	Br (4)–Hg (1)–Br (3)	102.176 (10)
Br (4)–Hg (1)–Br (2)	114.042 (11)	Br (1)–Hg (1)–Br (3)	101.330 (11)
Br (1)–Hg (1)–Br (2)	116.734 (13)	Br (2)–Hg (1)–Br (3)	91.901 (10)

intermolecular interactions				
interaction	H···A (Å)	D···A (Å)	D–H (Å)	>D–H···A (°)
N (1)–H (1N)···Br (3)	2.3852	3.202 (3)	0.880	154.53
N (2)–H (2N)···Br (2)	2.4593	3.276 (3)	0.880	154.60
C (1)–H (1)···Br (4)	2.7677	3.673 (4)	0.950	159.61
C (2)–H (2)···Br (1)	2.9689	3.800 (4)	0.951	146.85
C (4)–H (4)···Br (3)	2.9257	3.830 (3)	0.950	159.50
C (7)–H (7)···Br (1)	2.8372	3.751 (4)	0.950	132.27
C (8)–H (8)···Br (3)	2.9803	3.653 (3)	0.949	128.98
C (11)–H (11)···Br (2)	2.9828	3.834 (4)	0.950	149.89
C (12)–H (12)···Br (4)	2.8960	3.789 (4)	0.950	157.08

hydrogen bonds (WHB).[9] Despite being considered secondary interactions, the formation of the cations is deemed responsible to increase the hydrogen donor propensity of the aromatic C−H groups, thus promoting the formation of C−H···X (X = Cl, Br, or I) interactions. Likewise, it facilitated the formation of X···π interactions instead of C−H···π associations. All of them arise as determining factors in the structural analysis.

The essential interactions will be divided into three groups: N−H/C−H···X, X···Hg(II), and planar π···π interactions. For the sake of analyzing them, Hirshfeld surfaces with their 2D
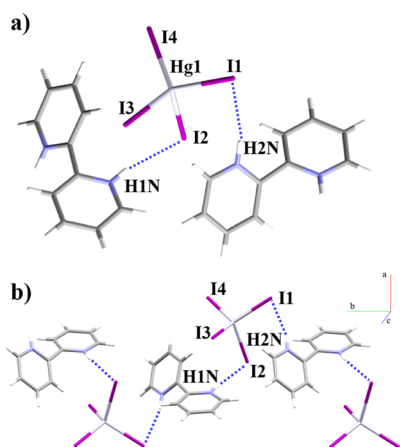
Figure 3. (a) Molecular structure of (2,2′-H₂bipy)(HgI₄) (**3**) highlighting the ionic interactions between the 2,2′-H₂bipy cations and the iodine atoms and (b) 1D *zigzag* association through the *b* axis.

Table 3. Selected Bond Lengths, Angles and Intermolecular Interactions of (2,2′-H₂bipy)(HgI₄) (3)

bond lengths (Å)			
Hg (1)−I (1)	2.8032(4)	Hg (1)−I (3)	2.7756 (5)
Hg (1)−I (2)	2.8398(5)	Hg (1)−I (4)	2.7483 (4)
bond angles (°)			
I (4)−Hg (1)−I (3)	116.276 (14)	I (4)−Hg (1)−I (2)	111.799 (14)
I (3)−Hg (1)−I (1)	111.401 (14)	I (3)−Hg (1)−I (2)	100.591 (14)
I (4)−Hg (1)−I (1)	108.793 (14)	I (1)−Hg (1)−I (2)	107.493 (13)

intermolecular interactions				
interaction	H⋯A (Å)	D⋯A (Å)	D−H (Å)	>D−H⋯A (°)
N (1)−H (1N)⋯I (2)	2.6524	3.486 (5)	0.880	158.38
N (2)−H (2N)⋯I (1)	2.5764	3.434 (5)	0.880	165.99
C (4)−H (4)⋯I (2)	3.1783	4.022 (6)	0.950	149.05
C (7)−H (7)⋯I (3)	3.1264	3.977 (6)	0.950	149.87
C (8)−H (8)⋯I (4)	3.1363	3.895 (7)	0.950	138.10
C (9)−H (9)⋯I (2)	3.1407	3.976 (6)	0.950	147.66

fingerprint plots and 3D deformation density (DD) maps have been generated using CrystalExplorer 17.5.[45] The DD

Table 4. Selected Bond Lengths and Angles of (1,10-Hphen)₂(HgCl₄)·H₂O (4), (1,10-Hphen)(HgBr₄) (5), and (1,10-Hphen)(HgI₄) (6)[a]

4		bond lengths (Å)	
Hg (1)−Cl (1)	2.4412 (5)	Hg (1)−Cl (3)	2.4803 (4)
Hg (1)−Cl (2)	2.5452 (5)	Hg (1)−Cl (4)	2.4952 (5)
bond angles (°)			
Cl (1)−Hg (1)−Cl (3)	115.258 (15)	Cl (1)−Hg (1)−Cl (2)	107.685 (16)
Cl (1)−Hg (1)−Cl (4)	115.283 (18)	Cl (3)−Hg (1)−Cl (2)	102.096 (15)
Cl (3)−Hg (1)−Cl (4)	108.624 (16)	Cl (4)−Hg (1)−Cl (2)	106.723 (18)
5		bond lengths (Å)	
Hg (1)−Br (1)	2.5594 (10)	Hg (1)−Br (3)	2.4512 (11)
Hg (1)−Br (2)	2.4486 (11)	Hg (1)−Br (4)	2.5221 (11)
bond angles (°)			
Br (2)−Hg (1)−Br (3)	120.59 (4)	Br (2)−Hg (1)−Br (1)	108.55 (4)
Br (2)−Hg (1)−Br (4)	110.75 (4)	Br (3)−Hg (1)−Br (1)	104.78 (4)
Br (3)−Hg (1)−Br (4)	108.41(4)	Br (4)−Hg (1)−Br (1)	102.02 (4)
6		bond lengths (Å)	
Hg (1)−I (1)#1	2.7760 (9)	Hg (1)−I (2)#1	2.7737 (9)
bond angles (°)			
I (2)−Hg (1)−I (2)#1	113.27 (4)	I (2)#1−Hg (1)−I (1)#1	105.36 (2)
I (2)−Hg (1)−I (1)#1	109.83 (2)	I (1)#1−Hg (1)−I (1)	113.36 (4)

[a]#1 −x + 2,y,−z.

isosurfaces of **1−5** are drawn at 0.008 eau⁻³, and their wave functions were calculated by the density functional theory (DFT) at the 6-311++G(2d,2p) level with Becke 88 gradient-corrected exchange and LYP correlation energy functional[46] using TONTO. Unfortunately, the structural disorder of compound **6** has excluded it from this calculation.

The DD mapping allows the representation of electronic density distribution along the molecule after suffering the polarization because of the interactions in which it participates. Low electron density areas termed charge depletion (CD) regions can attractively interact with charge concentration (CC) areas which are more electron rich. In this sense, univalent halogen atoms can be polarized upon coordination and generate a CD region named σ-hole[6,7] on the extension of the bond and thus more electron-rich regions at the sides.
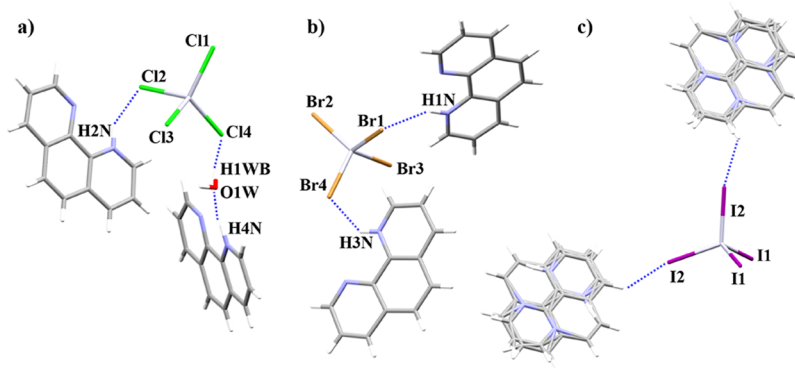

Figure 4. Molecular structure of (1,10-Hphen)₂(HgX₄) (X = (a) Cl (**4**), (b) Br (**5**), or (c) I (**6**)) highlighting the closer interactions between the 1,10-Hphen cations and the halogen atoms.

Table 5. Intermolecular Interactions of (1,10-Hphen)$_2$(HgCl$_4$)·H$_2$O (4)[a]

interaction	H···A (Å)	D···A (Å)	D-H (Å)	>D-H···A (°)
N (2)−H(2N)···Cl (2)	2.4169	3.200 (2)	0.880	148.44
N (4)−H(4N)···O (1 W)	1.855	2.683 (2)	0.880	155.87
O (1W)−H (1WB)···Cl (4)	2.375 (2)	3.171 (1)	0.803 (2)	171.16
C (2)−H (2)···Cl (1)	2.7057	3.576 (2)	0.950	152.60
C (3)−H (3)···Cl (3)	2.7647	3.661 (2)	0.950	157.57
C (13)−H (13)···Cl (4)	2.8201	3.461 (2)	0.950	125.62
C (14)−H (14)···Cl (2)	2.9070	3.647 (2)	0.950	135.66
C (18)−H (18)···Cl (1)	2.7230	3.669 (2)	0.950	173.71
C (21)−H (21)···Cl (4)	2.9302	3.727 (2)	0.950	142.24
π···π interactions				
Cg (1)···Cg (2)	3.685 Å			68.06°
Cg (3)···Cg (4)	3.593 Å			77.33°

[a]Cg (1): C4−C5−C6−C7−C11−C12; Cg (2): N1−C1−C2−C3−C4−C12; Cg (3): N4−C17−C18−C19−C20−C21; Cg (4): C16−C17−C20−C22−C23−C24.

Structures Containing (2,2′-Hbipy)$^+$ or (2,2′-H$_2$bipy)$^{2+}$ (1−3).

The N−H···X contacts hold together these arrays being the strongest interactions, subsequently supported by C−H···X associations. Their Hirshfeld surfaces outline these contacts, and the shorter N−H···X interactions are represented as sharp peaks in the 2D fingerprint plots (Figure 8).

The percentages of the surface area implied in these interactions are 31.5 and 28.8 (1), 42.6 (2), and 50.1 (3), being the greatest values compared to the rest (Table 8). The size of the halogen atoms and proximity to the cations are the main contributors; hence, even if 3 has a bigger percentage, the position of the peaks in the 2D fingerprint plots reflects the larger distances and thus weaker interactions between the inner hydrogens of the surface and the closest outer I atom.

The DD mapping of (2,2′-Hbipy)$^+$ (1) and (2,2′-H$_2$bipy)$^{2+}$ (2 and 3) displays large CD regions extended throughout the rings promoted by their protonation and the interactions with the surrounding atoms (Figure 9). Within this frame, the tendency of halogen atoms of being oriented through a side, perpendicular to the extension of the bond when they interact with CD regions, or through the extension of the bond when they associate to CC regions, suggests the presence of σ-hole interactions. It is worth mentioning a haptic-like interaction[2] between the face of the (HgI$_4$)$^{2−}$ tetrahedra and the pyridyl ring of the (2,2′H$_2$bipy)$^{2+}$ cation (Figure 9c), which could facilitate charge transfers (CTs) between them.

For what concerns the X···Hg(II) interactions, they have modified the nuclearity and association of inorganic anions between themselves, forming strong linear associated dimeric arrays (1), weak linear associated monomers (2), or discrete monomers assembled by cations in a zigzag fashion (3). Their 2D fingerprint displays small sharp peaks that decrease until disappearance from Cl to I, and the surface percentage between the halogen atoms and the Hg(II) centers being 3.8 (1), 1.8 (2), and 0.2 (3) thereby confirms the aforementioned tendency. Likewise, the distortion of the (HgX$_4$)$^{2−}$ (X = Cl, Br, or I) geometry is directly correlated to the strength of the interactions between the inorganic units in the order Cl > Br > I (Figure 8).
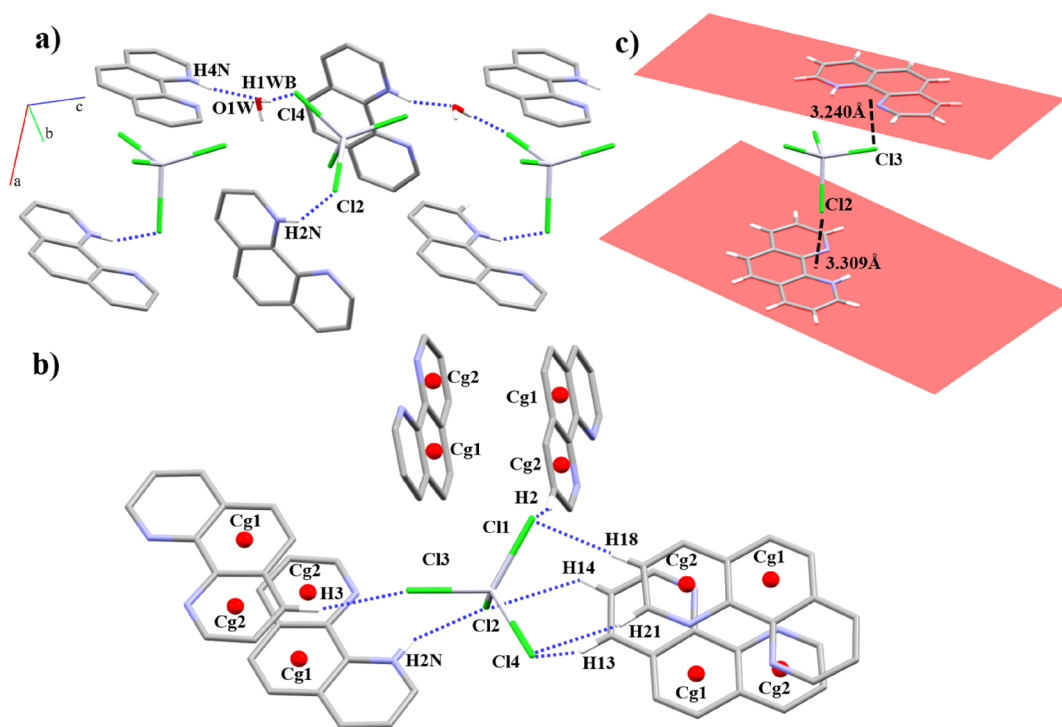

Figure 5. Intermolecular interactions of (1,10-Hphen)$_2$(HgCl$_4$)·H$_2$O (4). (a) *Zigzag* chains formed through N−H···Cl and N−H···O/O−H···Cl interactions. (b) Six (1,10-Hphen)$^+$ cations around (HgCl$_4$)$^{2−}$. Hydrogen atoms that do not interact with the anion are omitted for clarity. (c) Cl···π interactions. Dashed black lines pinpoint the distance of Cl to the plane containing the aromatic rings.

Table 6. Intermolecular Interactions of (1,10-Hphen)$_2$(HgBr$_4$) (5)^a

interaction	H⋯A (Å)	D⋯A (Å)	D−H (Å)	>D−H⋯A (°)	
N (1)−H(1N)⋯Br (1)	2.412	3.15 (1)	0.88	141.18	
N (3)−H(3N)⋯Br (4)	2.409	3.12 (1)	0.88	138.19	
C (1)−H (1)⋯Br (3)	2.753	3.61 (2)	0.95	150.05	
C (1)−H (1)⋯Br (1)	2.935	3.41 (1)	0.95	112.08	
C (2)−H (2)⋯Br (4)	2.982	3.71 (1)	0.95	133.91	
C (3)−H (3)⋯Br (1)	2.728	3.64 (1)	0.95	160.67	
C (6)−H (6)⋯Br (2)	2.863	3.78 (2)	0.95	163.42	
C (13)−H (13)⋯Br (4)	2.841	3.35 (2)	0.95	114.35	
C (13)−H (13)⋯Br (1)	2.647	3.52 (1)	0.95	153.50	
C (14)−H (14)⋯Br (2)	2.747	3.57 (1)	0.95	146.05	
C (15)−H (15)⋯Br (4)	2.539	3.47 (2)	0.95	165.58	
C (18)−H (18)⋯Br (3)	2.826	3.74 (2)	0.95	163.58	
π⋯π interactions					
Cg (1)⋯Cg (3)	3.621 Å	66.63°	Cg (2)⋯Cg (2)	3.613 Å	78.51°
Cg (3)⋯Cg (1)′	3.633 Å	65.28°			

^{a}Cg (1) = Cg (1)′: N3−C13−C14−C15−C16−C24; Cg (2): C16−C17−C18−C19−C23−C24; Cg (3): N4−C19−C20−C21−C22−C23.
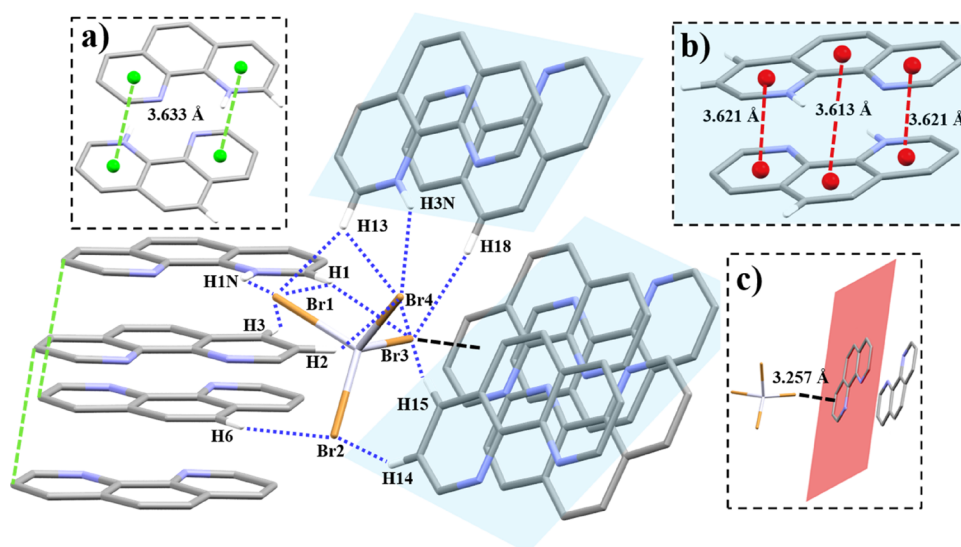

Figure 6. Intermolecular interaction of (1,10-Hphen)$_2$(HgBr$_4$) (5). Hydrogen atoms not involved in the interactions are omitted for clarity. Highlighting of (b) double or (b) triple π⋯π stacking. (c) Br⋯π contact. Dashed black lines pinpoint the distance of Br to the plane containing the aromatic rings.
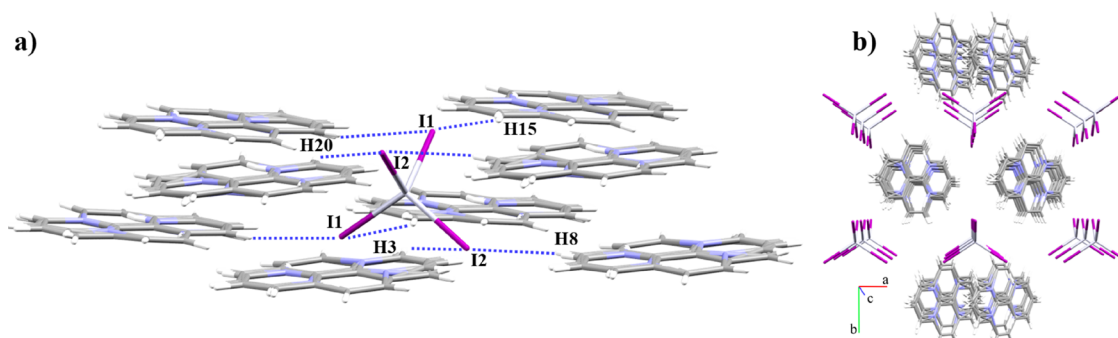

Figure 7. (a) Intermolecular interaction of (1,10-Hphen)$_2$(HgI$_4$) (6). (b) View of the piled packing of the anions or cations.

The smaller radius of Cl (1.75 Å) compared to Br (1.85 Å) and I (1.98 Å), in combination with its higher electronegativity, allowed the formation of dimeric units linearly assembled through semi-coordination bonds. In the case of Br, which is midway in size, there is a clear directional Hg(II)⋯Br interaction, out-of-bond range but enough to maintain the

linear disposition of the monomeric units. On the contrary, the bigger radius and lower electronegativity of I weaken this association and facilitate the distortion of the linear disposition. The intra-chain Hg(II)⋯Hg(II) distance increases in the order **1 > 2 > 3** being 4.3595 (4) Å, 6.3546 (5) Å, and 6.9656 (5) Å, respectively.

Table 7. Intermolecular Interactions of (1,10-Hphen)$_2$(HgI$_4$) (6)^a

interaction	H···A (Å)	D···A (Å)	D−H (Å)	>D−H···A (°)
C (3)−H (3)···I (2)	3.1712	3.913 (8)	0.951	136.25
C (8)−H (8)···I (2)	3.0707	3.844 (8)	0.950	136.70
C (15)−H (15)···I (1)	3.0829	3.871 (10)	0.950	141.30
C (20)−H (20)···I (1)	3.1712	3.913 (8)	0.950	136.25
π···π interactions				
Cg (1)···Cg (2)	3.750 Å			50.08°

^{a}Cg (1): N3−C13−C14−C15−C16−C24; Cg (2): C16−C17−C18−C19−C23−C24.

Since 2,2′-bipyridine tends to be in trans conformation and is not planar,[47] its diprotonation with the consequent positive charge repulsion probably emphasize it. Planarity decreased from mono- to diprotonation (rings torsion angle: 1.53 and 2.66° (**1**), 34.66° (**2**), and 51.74° (**3**)) and thus, π···π interactions are not favored in **2** and **3**. What should be noted is the nearly planar (2,2′-Hbipy)$^+$. The lone electron pair of the neighboring N atom could stabilize the pyridinium proton and retain the planarity, favoring the assembly of (2,2′-Hbipy)$^+$ cations through weak π···π interactions.

Structures Containing (1,10-Hphen)$^+$ (4−6). In compounds **4** and **5**, the Hirshfeld surface analysis with 2D fingerprint plot of N−H/C−H···X interactions (Figure 10) has similar distance values compared to that of **1−3**, the percentages of the surface being decreased (16.2 and 17.2 (**4**) and 22.5 and 22.7 (**5**)) because cations tend to interact between themselves by π···π interactions (Table 9).

The structural rigidity of (1,10-Hphen)$^+$ cations hinders the rotation of the rings and the consequent loss of planarity, and this structural feature promotes the formation of double or triple π···π interactions between the cations. Likewise, X···Hg(II) interactions are negligible, the percentage of the surface being 0.0.

The intra-chain Hg(II)···Hg(II) distance tendency in **4−6** is not in line with that observed in **1−3**, probably as a result of the spacing promoted by the presence of the water molecule in **4**, being 8.3158 (5), 7.8160 (7), and 8.911 (1) Å, respectively.

The DD maps of the cations in **4** and **5** exhibit a similar behavior of the N−H/C−H···X interactions, suggesting the presence of halogen σ-holes but in this case, the polarization over the aromatic H atoms of the cations has bigger CC regions. The (1,10-Hphen)$^+$ cations are close between them probably because they are bulkier and thus, the proximity of the positively charged N−H$^+$ from neighboring cations promotes the formation of these CC regions (Figure 11). Halogen atoms are likely to interact with electron-deficient π systems over the periphery of the rings.[4,5] Figure 11a,c illustrates the Cl···π and Br···π interactions, respectively. In both, the halogen atoms are directed to the periphery of the (1,10-Hphen)$^+$ rings at a distance of 3.512 (2) Å (Cl (3)···C (17)) and 3.383 (2) Å (Cl (3)···C (16)) in **4** or at 3.36 (1) Å (Br (3)···N (3)) and 3.39 (2) Å (Br (3)···C (13)) in **5**. This preferential orientation has a more electrostatic character, and it has been proven to promote CTs between the halogen atom and the electron-deficient π system.[5]

Overall, the (1,10-Hphen)$^+$ retention of planarity promoted the formation of layered crystal structures increasingly from **4** to **6** (Figure 12). Withal, the planarity of (2,2′-Hbipy)$^+$ in **1** resulted in an intermediate packing being the cations with similar disposition to the structures of **4−6** but without the formation of layers. Finally, the trans conformation of (2,2′-H$_2$bipy)$^{2+}$ in **2** and **3** leads to the worst cation···cation
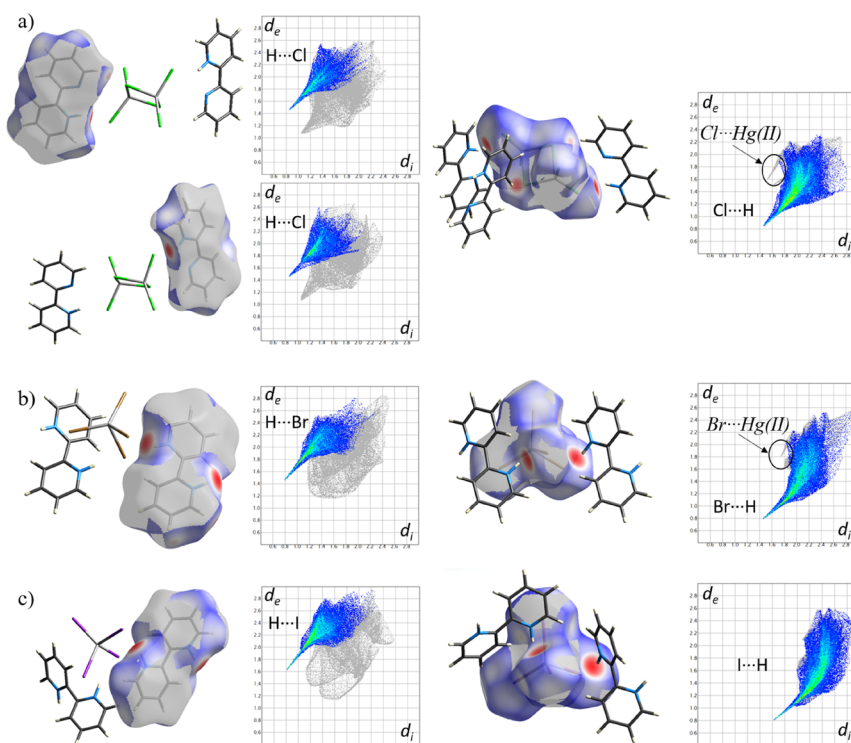

Figure 8. Hirshfeld surface representation and 2D fingerprint plot of the organic cations (left) and inorganic anions (right) of compounds (a) (2,2′-Hbipy)$_2$(Hg$_2$Cl$_6$) (**1**), (b) (2,2′-H$_2$bipy)(HgBr$_4$) (**2**), and (c) (2,2′-H$_2$bipy)(HgI$_4$) (**3**).

Table 8. Percentage (%) of Hirshfeld Surface Implied in Each Interaction for Compounds 1−3 (X = Cl (1), Br (2), and I (3))

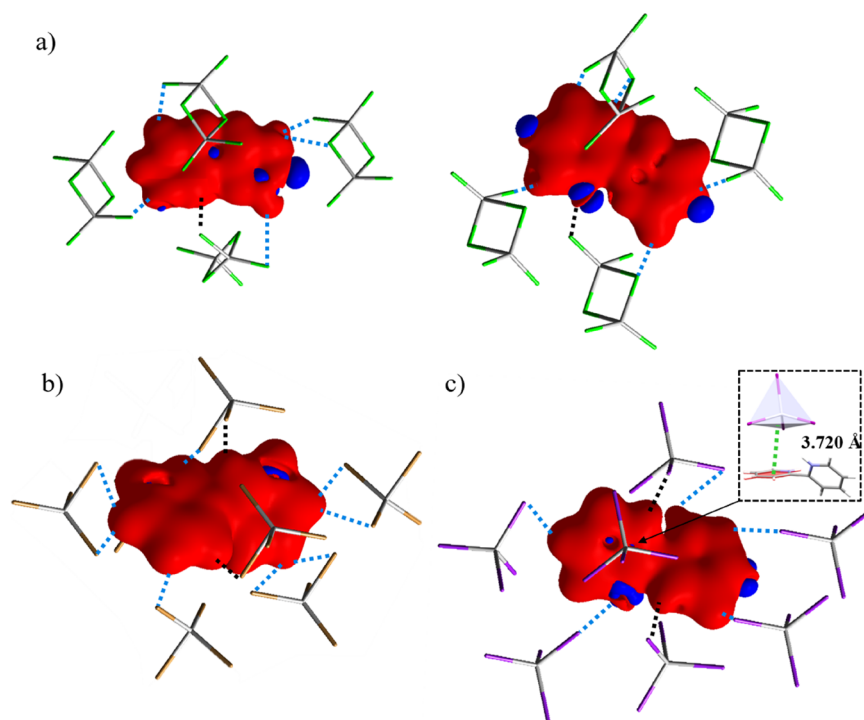|	inorganic anions				organic cations		
interaction	1	2	3	interaction	1	2	3
X⋯Hg(II)	3.0	1.5	0.1	N⋯X	1.0	3.0	3.0	3.0
X⋯X	2.2	7.9	4.1	H⋯X	31.5	28.8	42.6	50.1
X⋯N	2.2	3.4	2.8	C⋯C	8.0	8.2	3.4	1.7
X⋯C	6.0	8.9	10.3	C⋯X	3.7	3.1	7.0	9.7
X⋯H	78.3	73.4	78.7				
Hg⋯X	3.8	1.8	0.2				

Figure 9. 3D deformation density maps of compounds (a) **1**, (b) **2**, and (c) **3** highlighting CD (red) and CC (blue) regions. Dashed black lines indicate N−H⋯X contacts, while dashed blue lines highlight C−H⋯X interactions (X = Cl (**1**), Br (**2**), and I (**3**)). In detail, haptic-like interaction in panel (c). The isosurfaces are drawn at 0.008 eau^{-3}.

interaction and the intersperse distribution of the anions and cations.

Electronic Structure Analysis of 1−6. With the aim of analyzing the electronic structure and the effect of halide and organic cation on the band gap of the six salts, PBE-D2[48,49] periodic boundary calculations using the VASP code[50,51] were performed (see details in the Experimental Section). The projected density of states (pDOS) of the six compounds around the Fermi level are shown in Figure 13a−f. In this figure, we report the total DOS (black curves) and the contributions arising from Hg(II) centers (red curve), the halogen atoms (green curve), and the organic cations (blue curve). Noteworthily, the pDOS reports the number of electronic states at a given energy, thus defining the electronic bands of the compounds and the corresponding band gap.

For all compounds, the conducting band is mainly composed of the p orbitals of the organic cation, the contribution of Hg(II) and the halide atom being always small. In particular, the contribution of the organic cation to this conducting band shows less pronounced peaks for **5** and **6**. This suggests a larger electronic delocalization, which could be associated with a stronger π⋯π interaction between the organic cations in these two salts. Instead, the composition of the

valence band shows larger variations. Within this frame, all compounds show an important contribution of the p orbitals of the halogen atom, the peaks for **5** (Figure 13e) and **6** (Figure 13f) being sharper where no inorganic−inorganic interactions are identified. However, in (1,10-Hphen)$^+$ and/or chlorine-containing salts (Figure 13a,d−f), the contributions to the valence band of p orbitals from the organic cation are not neglectable.

This is particularly remarkable for **4** where the highest in energy occupied states are mainly composed of (1,10-Hphen)$^+$ p orbitals. Therefore, the most likely excitations are expected to involve charge-transfer processes for bromine and iodine salts while for chlorine species, the charge-transfer character of the main excitations is expected to be smaller, particularly for **4**.

The gap between the valence and conducting band is also highly dependent on the halide anion and, in a smaller extent, by the organic cation. In this context, chlorine-containing salts (**1** and **4**) show the largest band gaps. Moreover, within those compounds having the same organic cation, it decreases from chlorine to iodine. These results are consistent with the color of the synthetized solids: **1**, **4**, and **5** are white; **2** is pale yellow; and **3** and **6** are yellow. It may seem that the organic cation
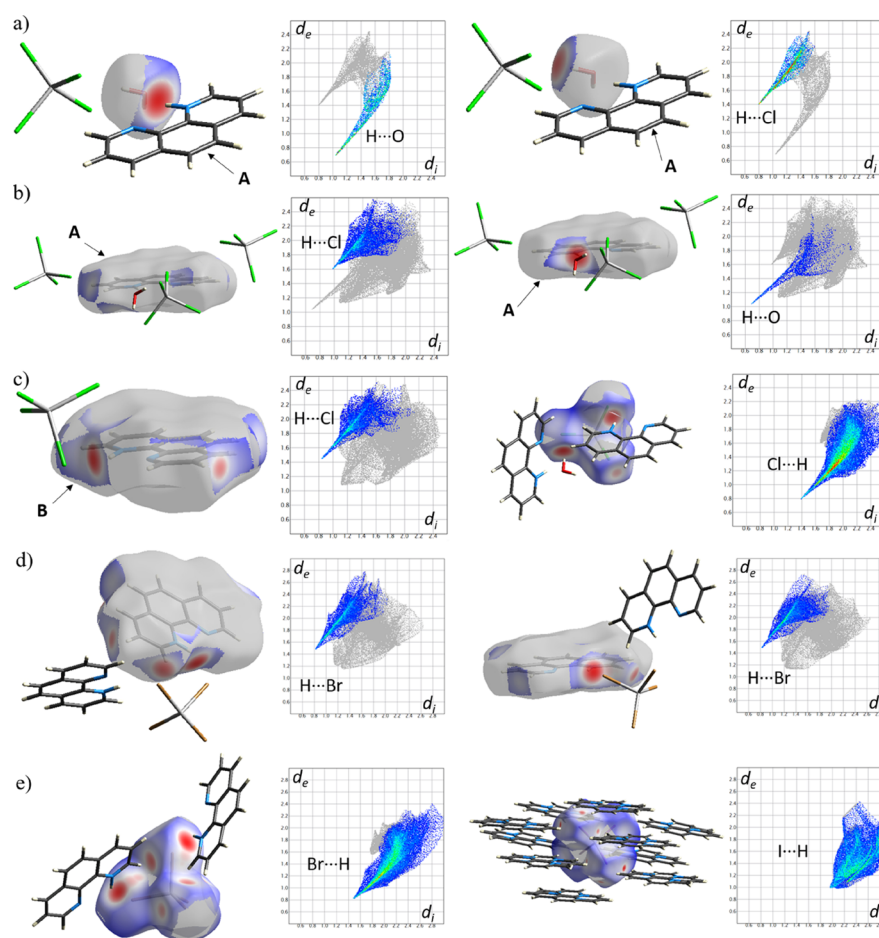
Figure 10. Hirshfeld surface and 2D fingerprint plot representations of (a) water molecule in **4**; (b) (1,10-Hphen)⁺ associated with water in **4**, appointed as *A*; (c) (1,10-Hphen)⁺ associated with (HgCl₄)²⁻ appointed as *B* (left) and (HgCl₄)²⁻ anion in **4** (right); (d) two different (1,10-Hphen)⁺ in **5**; and (e) (HgBr₄)²⁻ (left) (**5**) and (HgI₄)²⁻ (right) (**6**) anions.

Table 9. Percentage (%) of Hirshfeld Surface Implied in Each Interaction for Compounds 4−6 (X = Cl (4), Br (5), and I (6))[a]

	inorganic anions			organic cations					
interaction	**4**	**5**	**6**	interaction	**4**			**5**	
X···Hg(II)	0.0	0.0	0.0		*A*	H₂O	*B*		
X···X	0.0	0.0	0.9	N···X	1.0	0.0	2.0	0.9	1.0
X···N	3.9	2.4	0.1	H···X	16.2	33.4	17.2	22.5	22.7
X···C	9.0	8.3	4.1	C···C	7.7	0.0	7.5	10.5	4.7
X···H	83.0	85.6	90.9	C···X	5.3	0.0	4.2	3.0	3.2
Hg···X	0.0	0.0	0.0	O···H	0.0	27.6	0.0	0.0	0.0

[a]For identification of *A* and *B* see Figure 1010ca-.

nature has almost no effect on the band gap per se. However, since it has a big influence on the crystal packing, it can indirectly modify the band gap. This is particularly the case of complexes **2** and **5** that only differ on the organic cation, and they present very different band gaps (Figure 13b,e). Indeed, these two complexes show very different packing and intermolecular interactions, which appears to be the origin of this large difference between their band gaps.

In summary, optical properties of these compounds are associated with charge-transfer processes from the halogen atoms to the organic cations being more pronounced for bromine- and iodine-containing compounds. The energy difference between the valence and conducting band is largely influenced by the halogen, decreasing the band gap as Cl > Br > I. In this set of compounds, the organic cation has directly

little influence on the band gap of the different salts, but as clearly suggested for the bromine-containing compounds (**2** and **5**), it is capable of indirectly modifying the band gap through its effect on the crystal packing.

■ CONCLUSIONS

A series of six Hg(II) halides (Cl, Br, and I) with aromatic conjugated (2,2′-Hbipy)⁺, (2,2′-H₂bipy)²⁺ and (1,10-Hphen)⁺ cations have been synthesized. The study of their crystal structures enabled the identification of the intermolecular interactions and revealed their effect on the final packing. The small size and electronegativity of chlorine promoted a shorter anion···anion intra-chain distance than Br and I. In this regard, the bulkiness of the (1,10-Hphen)⁺ cations does not
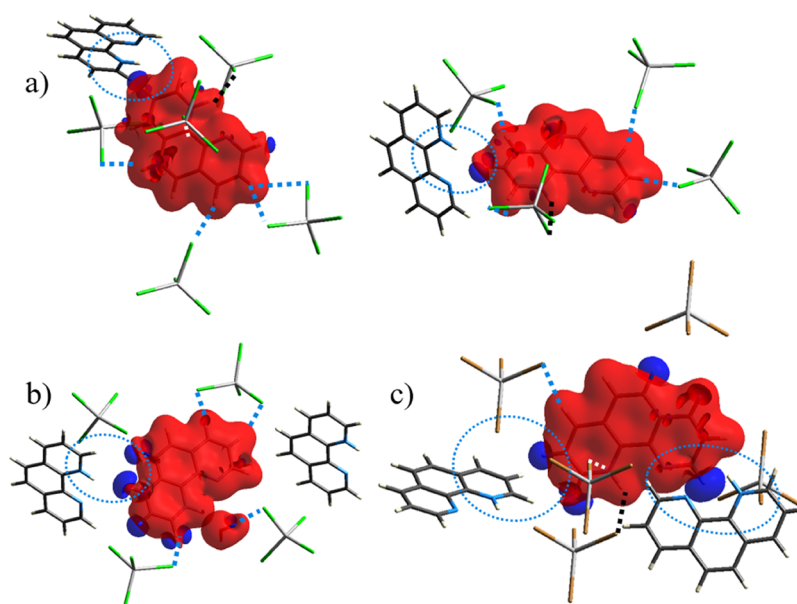
Figure 11. 3D deformation density maps highlighting CD (red) and CC (blue) regions of (a) (1,10-Hphen)$^+$···Cl and (b) (1,10-Hphen)$^+$···H$_2$O associated in **4** and (c) (1,10-Hphen)$^+$···Br associated in **5**. Dashed black lines indicate N−H···X contacts, dashed blue lines highlight C−H/O−H···X interactions, and dashed white lines identify X···π interactions. Dashed blue circles point large CC regions. The isosurfaces are drawn at 0.008 eau^{-3}.
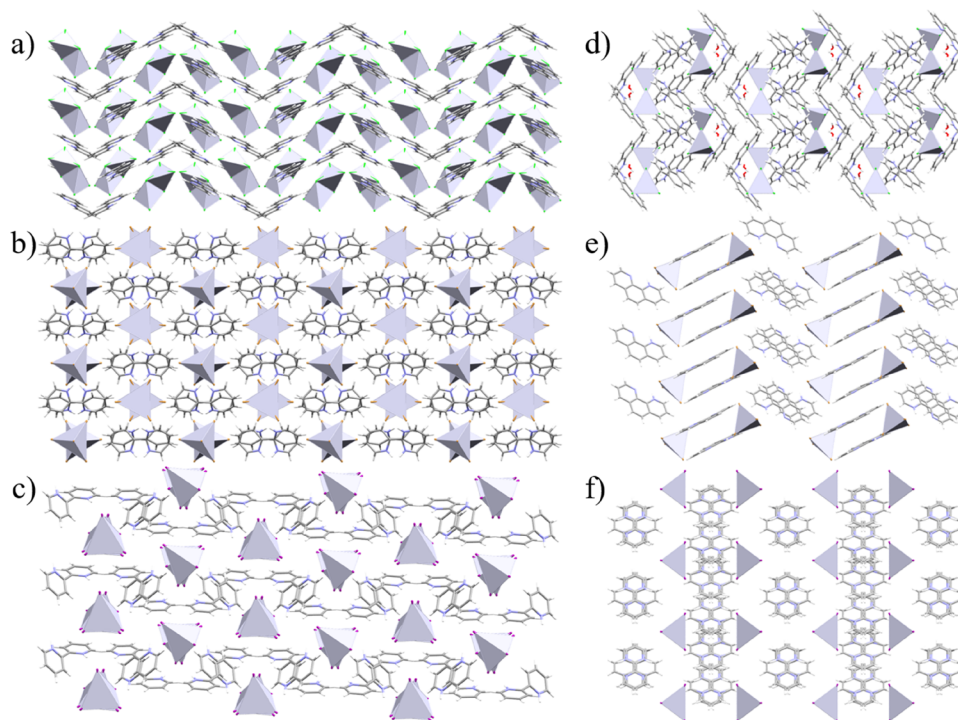

Figure 12. *c* axis view of the crystal packing in (a−f) compounds **1−6**, respectively.

particularly increase this spacing but instead lengthens the anion···anion inter-chain distance located at the sides of these chains. In addition, their planarity promoted the stacking of the ring, shortening the cation···cation distance. The electronic structure calculations revealed the p orbitals of the organic cations as main contributors to the conducting band, while those of the halides defined the valence band. The electron transport in **1−6** is expected to involve charge-transfer processes favored in **2**, **3**, **5**, and **6** where the band gap falls within the appropriate range for their potential application as

light absorbers. Despite the band gap being highly dependent on the halide and following the series Cl > Br > I, the modification of the crystal packing by the cations can substantially vary it. This has been evinced in the pair of compounds **2** and **4**, in which the better organic−inorganic interactions in **2** promoted a smaller band gap.

■ EXPERIMENTAL SECTION

Chemical Risks. Any mercury compound poses potential health risks, and appropriate safety precautions along with
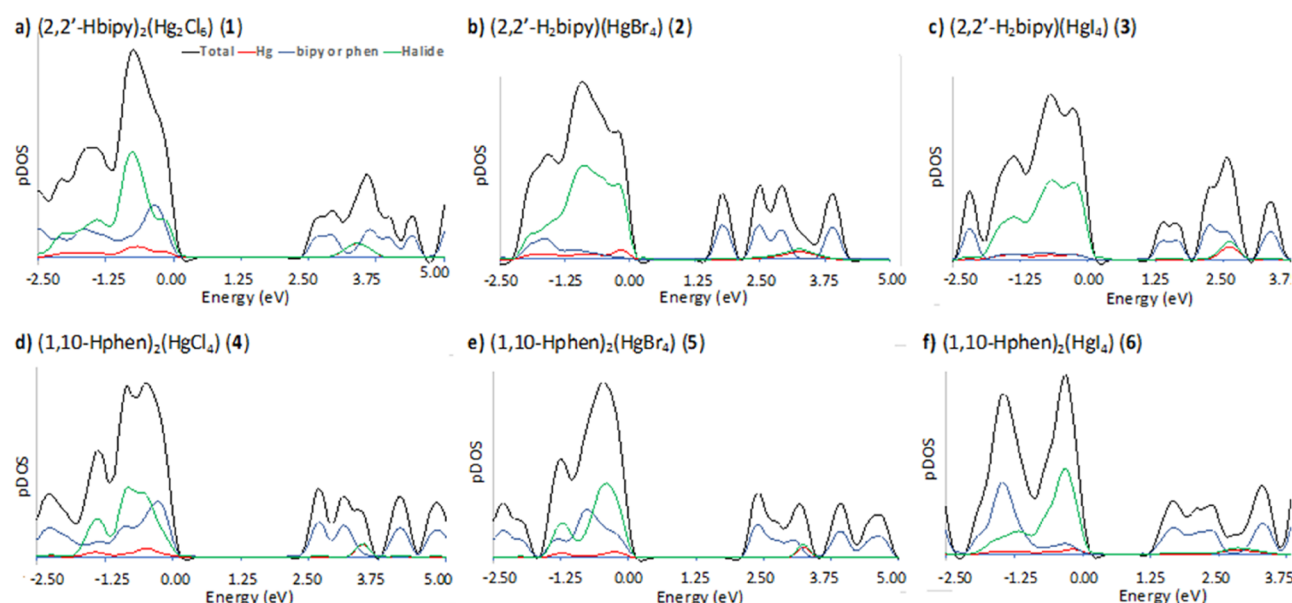
Figure 13. Projected density of states (pDOS) of the six compounds. Energies are referred to the Fermi level. The total (black curve) DOS is decomposed in those states arising from Hg(II) (red curve), the organic cation (blue curve), and the halogen atoms (green curve).

disposal procedures must be taken in handling the complexes reported here. Hg(II) halides sublime to emit highly poisonous fumes and must be handled only under appropriate conditions.

Materials and Methods. Hg(II) halides ($HgCl_2$, $HgBr_2$, and HgI_2), 2,2′-bipyridine (2,2′-bipy), 1,10-phenanthroline monohydrate (1,10-phen), methanol (MeOH), and dichloromethane (CH_2Cl_2) solvents as well as hydrobromic acid (HBr, 48 wt. %) and hydroiodic acid (HI, 57 wt. %) were purchased from Sigma-Aldrich. Hydrochloric acid (HCl, 37 wt. %) was purchased from Scharlau. DMSO-d_6 was used for the ^1H NMR experiments and was purchased from Eurisotop. All of them were used without further purification. Elemental analyses (C, H, and N) were carried out on a Thermo Scientific Flash 2000 CHNS analyzer. PXRD patterns were recorded at 298 K on a PANalytical X′Pert PRO MPD θ/θ powder diffractometer of 240 mm radius in a configuration of a convergent beam with a focalizing mirror and a transmission geometry with flat samples sandwiched between low absorbing films from 2 to 30° with a step size of 0.0263° and a measuring time of 300s per step. The samples were sandwiched between films of polyester Mylar of 3.6 μm of thickness. FTIR-ATR spectra were recorded on a Perkin Elmer spectrometer equipped with a universal attenuated total reflectance (ATR) accessory with a diamond window in the range 4000–500 cm^{-1}. ^1H NMR spectra were recorded on an NMR-FT Bruker360 MHz spectrometer in DMSO-d_6 solution at room temperature (r.t.). All chemical shifts (δ) are given in ppm relative to TMS as the internal standard. Simultaneous TG/DTA determinations were carried out in a Netzsch STA 409 instrument with an aluminum oxide powder (Al_2O_3) crucible and heating at 5 °C·min^{-1} from 20 to 400 °C under a nitrogen atmosphere with a flow rate of 80 mL· min^{-1}. Al_2O_3 (PerkinElmer 0419-0197) was used as a standard. Further experimental data and PXRD, FTIR-ATR and ^1H NMR spectra, and TG/DTA determinations of **1–6** are in the Supporting Information (Figures S1–S14).

Synthesis of Complexes 1–6. A methanolic solution (7 mL) of $HgCl_2$ (0.151 g, 0.557 mmol) was added dropwise to a CH_2Cl_2 solution (14 mL) of 2,2′-bipy (0.173 g, 1.11 mmol) with 0.2 mL of aqueous HCl (37 wt %). The solution was let

to evaporate slowly for 1 day until suitable crystals for single-crystal X-ray diffraction were grown. The solution was filtered off, and the resulting crystals were washed twice with cold dichloromethane (10 mL) and diethyl ether (10 mL) and dried under vacuum.

The syntheses of **2−6** were performed by the same methodology but using the corresponding acid (HBr or HI) and allowing to slowly evaporate for 1 day (**3** and **4**), 2 days (**2** and **5**), or 3 days (**6**).

1: Yield: 0.207 g (40%). Elem. anal. calc. for $C_{20}H_{18}Hg_2N_4Cl_6$ (928.28 g/mol): C, 25.88; H, 1.95; N, 6.04. Found: C, 25.63; H, 1.84; N, 6.04. FTIR-ATR (wavenumber, cm^{-1}): 3236 (w), 3150 (w), 3031 (m) [ν_{ar}(C–H)], 2932–2322(m) [ν(N–H)], 1600 (s) [ν(C= C/C=N)], 1524 (s) [ν(C=C/C=N)], 1447 (m) [ν(C=C/ C=N)], 1387 (s) [δ(C=C/C=N)], 1285 (s), 1242 (m), 1165 (w) [δ_{ip}(C–H)], 999 (w), 930 (w) [γ(N–H)], 802 (w), 760 (s) [δ_{oop}(C–H)], 623 (w), 541 (w). ^1H NMR (360 MHz; DMSO-d_6; 298 K, TMS): δ = 4.80 [br, N–H], 7.87 [2H, m, meta-H], 8.41 [2H, m, para-H], 8.66 [2H, t, ^3J = 7.3 Hz, C− C=C−H], 8.88 [2H, d, ^3J = 4.2 Hz, ortho-H].

2: Yield: 0.209 g (74%). Elem. anal. calc. for $C_{10}H_{10}HgN_2Br_4$ (678.41 g/mol): C, 17.70; H, 1.49; N, 4.13. Found: C, 17.62; H, 1.42; N, 4.08. FTIR-ATR (wavenumber, cm^{-1}): 3373 (br) [ν(N–H)], 3232 (w), 3138–3023 (m) [ν_{ar}(C–H)], 2983– 2631 (m) [ν(N–H)], 1599 (s) [ν(C=C/C=N)], 1563 (w), 1542 (w), 1523 (s) [ν(C=C/C=N)], 1473 (w), 1443 (m) [ν(C=C/C=N)], 1411 (w), 1385 (m) [δ(C=C/C=N)], 1281 (m), 1240 (m), 1167 (w) [δ_{ip}(C–H)], 1088 (w), 1073 (w), 1040 (w), 1014 (w), 997 (w), 940 (w), 920 (m) [γ(N– H)], 871 (w), 860 (w), 791 (w), 753 (s) [δ_{oop}(C–H)], 735 (s) [δ_{oop}(C–H)], 714 (m), 623 (m), 538 (m). ^1H NMR (360 MHz; DMSO-d_6; 298 K, TMS): δ = 5.32 [br, N–H], 7.88 [2H, dd, ^3J = 7.9 Hz, ^3J = 5.0 Hz, meta-H], 8.42 [2H, td, ^3J = 7.9 Hz, ^4J = 2.0 Hz, para-H], 8.66 [2H, d, ^3J = 8.1 Hz, C−C= C−H], 8.89 [2H, dd, ^3J = 5.1 Hz, ^4J = 1.7 Hz, ortho-H].

3: Yield: 0.152 g (53%). Elem. anal. calc. for $C_{10}H_{10}HgN_2I_4$ (866.41 g/mol): C, 13.86; H, 1.16; N, 3.23. Found: C, 13.67; H, 1.05; N, 3.11. FTIR-ATR (wavenumber, cm^{-1}): 3209 (br)

[ν(N–H)]/[ν(O–H)], 3091–3050 (m) [ν$_{ar}$(C–H)], 2945 (w), 2882 (w), 1627 (w), 1617 (w), 1582 (s) [ν(C=C/C=N)], 1569 (w), 1525 (s) [ν(C=C/C=N)], 1470 (w), 1457 (m) [ν(C=C/C=N)], 1428 (s) [δ(C=C/C=N)], 1411 (w), 1354 (w), 1326 (m), 1311 (w), 1277 (w), 1247 (w), 1215 (m), 1178 (m) [δ$_{ip}$(C–H)], 1150 (w), 1110 (w), 1089 (m), 1066 (w), 1037 (w), 1005 (w), 994 (w), 977 (w), 927 (m), 917 (m) [γ(N–H)], 861 (w), 809 (w), 754 (s) [δ$_{oop}$(C–H)], 737 (m) [δ$_{oop}$(C–H)], 720 (s) [δ$_{oop}$(C–H)], 644 (w), 633 (w), 611 (w), 541 (w). ^{1}H NMR (360 MHz; DMSO-d_6; 298 K, TMS): δ = 4.73 [br, N–H], 7.81 [2H, d, ^3J = 6.3 Hz, meta-H], 8.34 [2H, d, ^3J = 7.9 Hz, para-H], 8.61 [2H, d, ^3J = 8.3 Hz, C–C=C–H], 8.85 [2H, d, ^3J = 4.7 Hz, ortho-H].

4: Yield: 0.127 g (32%). Elem. anal. calc. for C$_{24}$H$_{20}$HgN$_4$Cl$_4$O (722.83 g/mol): C, 39.88; H, 2.79; N, 7.75. Found: C, 39.77; H, 2.71; N, 7.64. FTIR-ATR (wavenumber, cm^{-1}): 3178–2643 (br) [ν(O–H/N–H)], 3090–3022 (m) [ν$_{ar}$(C–H)], 2994 (w), 2948 (w), 1633 (w), 1613 (m), 1595 (m) [ν(C=C/C=N)], 1537 (s) [ν(C=C/C=N)], 1495 (w), 1464 (m) [ν(C=C/C=N)], 1452 (m) [ν(C=C/C=N)], 1415 (m) [δ(C=C/C=N)], 1365 (w), 1338 (w), 1315 (w), 1279 (m), 1234 (m), 1185 (m) [δ$_{ip}$(C–H)], 1152 (w), 1139 (w), 1098 (w), 1071 (w), 1043 (w), 1034 (w), 1007 (w), 987 (w), 916 (w) [γ(N–H)], 883 (w), 844 (s) [δ$_{oop}$(C–H)], 819 (m) [δ$_{oop}$(C–H)], 802 (sh.) [δ$_{oop}$(C–H)], 771 (s) [δ$_{oop}$(C–H)], 714 (s) [δ$_{oop}$(C–H)], 678 (w), 621 (m), 597 (w), 552 (w), 538 (w), 502 (w). ^{1}H NMR (360 MHz; DMSO-d_6; 298 K, TMS): δ = 4.10 [br, N–H], 8.20 [4H, dd, ^3J = 8.2 Hz, ^3J = 4.9 Hz, meta-H], 8.34 [4H, s, phenyl-H], 9.05 [4H, dd, ^3J = 8.2 Hz, ^4J = 1.6 Hz, para-H], 9.29 [4H, dd, ^3J = 4.9 Hz, ^4J = 1.5 Hz, ortho-H].

5: Yield: 0.271 g (74%). Elem. anal. calc. for C$_{24}$H$_{18}$HgN$_4$Br$_4$ (882.65 g/mol): C, 32.66; H, 2.06; N, 6.35. Found: C, 32.48; H, 1.94; N, 6.13. FTIR-ATR (wavenumber, cm^{-1}): 3193–3172 (m) [ν(N–H)], 3099–3040 (w) [ν$_{ar}$(C–H)], 1635 (w), 1613 (m), 1597 (m) [ν(C=C/C=N)], 1542 (s) [ν(C=C/C=N)], 1494 (m), 1464 (s) [ν(C=C/C=N)], 1451 (m), 1417 (m) [δ(C=C/C=N)], 1370 (m) [δ(C=C/C=N)], 1336 (m), 1314 (m), 1285 (m), 1242 (m), 1225 (m), 1182 (w) [δ$_{ip}$(C–H)], 1148 (w), 1097 (w), 1071 (w), 1032 (w), 960 (w) [γ(N–H)], 883 (w), 866 (w), 840 (s) [δ$_{oop}$(C–H)], 807 (s) [δ$_{oop}$(C–H)], 794 (m) [δ$_{oop}$(C–H)], 755 (s) [δ$_{oop}$(C–H)], 714 (s) [δ$_{oop}$(C–H)], 615 (m), 529 (m). ^{1}H NMR (360 MHz; DMSO-d_6; 298 K, TMS): δ = 4.24 [br, N–H], 8.22 [4H, dd, ^3J = 8.2 Hz, ^3J = 4.9 Hz, meta-H], 8.36 [4H, s, phenyl-H], 9.07 [4H, dd, ^3J = 8.2 Hz, ^4J = 1.2 Hz, para-H], 9.31 [4H, dd, ^3J = 4.8 Hz, ^4J = 1.2 Hz, ortho-H].

6: Yield: 0.255 g (72%). Elem. anal. calc. for C$_{24}$H$_{18}$HgN$_4$I$_4$ (1039.74 g/mol): C, 26.87; H, 1.69; N, 5.23. Found: C, 26.65; H, 1.52; N, 5.04. FTIR-ATR (wavenumber, cm^{-1}): 3448 (br) [ν(N–H)], 3094–3052 (w) [ν$_{ar}$(C–H)], 2980 (w), 2942 (w), 2869 (w), 2784 (w), 2738 (w), 2660 (w), 1634 (w), 1614 (m), 1593 (s) [ν(C=C/C=N)], 1541 (s) [ν(C=C/C=N)], 1493 (m) [ν(C=C/C=N)], 1467 (m), 1447 (m), 1414 (m) [δ(C=C/C=N)], 1378 (s) [δ(C=C/C=N)], 1335 (m), 1314 (m), 1287 (m), 1240 (m), 1221 (w), 1189 (w) [δ$_{ip}$(C–H)], 1147 (w), 1136 (w), 1098 (w), 1072 (w), 1029 (w), 993 (w), 964 (w) [γ(N–H)], 934 (w) [γ(N–H)], 883 (w), 840 (s) [δ$_{oop}$(C–H)], 823 (m) [δ$_{oop}$(C–H)], 807 (sh.) [δ$_{oop}$(C–H)], 767 (m) [δ$_{oop}$(C–H)], 714 (s) [δ$_{oop}$(C–H)], 618 (m), 599 (w), 541 (m), 518 (m). ^{1}H NMR (360 MHz; DMSO-d_6; 298 K): δ = 4.39 [br, N–H], 8.23 [4H, dd, ^3J = 8.7 Hz, ^3J = 4.7 Hz, meta-H], 8.36 [4H, s, phenyl-H], 9.07 [4H, d, ^3J = 8.3 Hz, para-H], 9.30 [4H, d, ^3J = 5.1 Hz, ortho-H].

X-Ray Crystallographic Data and Electronic Calculations. Colorless (**1**, **4**, and **5**), yellow (**3**), and red (**6**) prism-like or colorless plate-like (**2**) specimens were used for the X-ray crystallographic analysis. For all compounds, the frames were integrated with the Bruker SAINT software package using a narrow-frame algorithm (Tables 10 and 11).

The electronic structure of **1–6** has been analyzed by performing periodic DFT calculations using the VASP code.[50,51] All calculations were done at the PBE level of theory.[48] van der Waals interactions were included through Grimme's D2 empirical correction.[49] The use of D2 instead of D3 correction was based on previous results that showed that

Table 10. Crystal Structure Refinement Data for Compounds 1−3

parameters	1	2	3
empirical formula	C$_{20}$H$_{18}$Cl$_6$Hg$_2$N$_4$	C$_{10}$H$_{10}$Br$_4$HgN$_2$	C$_{10}$H$_{10}$I$_4$HgN$_2$
formula weigh	928.26	678.43	866.39
T (K)	100(2)	100(2)	100(2)
wavelength (Å)	0.71073	0.71073	0.71073
system, space group	monoclinic, P2$_1$/c	monoclinic, P2$_1$/c	monoclinic, P2$_1$/c
unit cell dimensions			
a (Å)	7.4413(3)	8.4640(6)	7.8704(4)
b (Å)	21.6102(12)	14.0128(10)	15.6908(7)
c (Å)	15.4817(8)	12.6748(8)	13.8093(7)
β (°)	94.962(2)	99.102(2)	90.282(2)
V (Å^3)	2480.3(2)	1484.36(18)	1705.33(14)
Z	4	4	4
D$_{calc}$ (g cm^3)	2.486	3.036	3.375
μ (mm^{-1})	13.029	21.116	16.250
F(000)	1712	1216	1504
crystal size (mm^3)	0.213 × 0.089 × 0.030	0.330 × 0.233 × 0.088	0.075 × 0.065 × 0.041
hkl ranges	−10 ≤ h ≤ 10	−10 ≤ h ≤ 10	−11 ≤ h ≤ 9
	0 ≤ k ≤ 30	0 ≤ k ≤ 17	−22 ≤ k ≤ 22
	0 ≤ l ≤ 22	0 ≤ l ≤ 15	−18 ≤ l ≤ 19
2θ range (°)	2.748−30.532	2.182−26.426	2.895−30.547
reflections collected/ unique/[R$_{int}$]	7586/7586/[R$_{int}$] = 0.0502	3019/3019/[R$_{int}$] = 0.0536	33,327/5178/ [R$_{int}$] = 0.0304
completeness to θ (%)	99.9	99.0	99.5
absorption correction	semi-empirical	semi-empirical	semi-empirical
max. and min. transmis.	0.7461 and 0.5426	0.7454 and 0.2515	0.7461 and 0.5031
refinement method	full matrix least-squares on |F|^2	full matrix least-squares on |F|^2	full matrix least-squares on |F|^2
data/restrains/ parameters	7586/0/289	3019/0/154	5178/0/154
goodness of fit (GOF) on |F|^2	1.066	1.063	1.254
final R indices [I > 2σ(I)]	R$_1$ = 0.0224, wR$_2$ = 0.0437	R$_1$ = 0.0228, wR$_2$ = 0.0545	R$_1$ = 0.0279, wR$_2$ = 0.0584
R indices (all data)	R$_1$ = 0.0340, wR$_2$ = 0.0503	R$_1$ = 0.0238, wR$_2$ = 0.0550	R$_1$ = 0.0390, wR$_2$ = 0.0659
extinction coefficient	n/a	n/a	n/a
largest diff. peak and hole (e Å^{-3})	1.542 and −1.644	1.408 and −2.586	1.663 and −1.871

Table 11. Crystal Structure Refinement Data for Compounds 4−6

parameters	4	5	6
empirical formula	$C_{24}H_{20}Cl_4HgN_4O$	$C_{24}H_{18}Br_4HgN_4$	$C_{24}H_{18}I_4HgN4$
formula weigh	722.83	882.65	1070.61
T (K)	100(2)	100(2)	100(2)
wavelength (Å)	0.71073	0.71073	0.71073
system, space group	monoclinic, $P2_1/c$	triclinic, P-1	monoclinic, $P2/m$
unit cell dimensions			
a (Å)	16.3186(6)	7.8160(7)	8.991(3)
b (Å)	10.6960(4)	9.0601(8)	19.040(8)
c (Å)	14.6085(5)	18.7870(17)	9.004(3)
α (°)	90	86.438(3)	90
β (°)	107.8560(10)	86.462(3)	93.322 (13)
γ (°)	90	66.489(3)	90
V (Å^3)	2427.00(15)	1216.59(19)	1538.8(10)
Z	4	2	2
D_{calc} (g cm^3)	1.978	2.409	2.311
μ (mm^{-1})	6.809	12.916	9.031
$F(000)$	1392	820	964
Crystal size (mm^3)	0.447 × 0.417 × 0.360	0.372 × 0.149 × 0.137	0.360 × 0.179 × 0.057
hkl ranges	$-23 \leq h \leq 22$	$-11 \leq h \leq 11$	$-12 \leq h \leq 12$
	$0 \leq k \leq 15$	$-12 \leq k \leq 12$	$-26 \leq k \leq 27$
	$0 \leq l \leq 20$	$0 \leq l \leq 26$	$-11 \leq l \leq 12$
2θ range (°)	2.312–30.522	2.454–30.589	2.506–30.516
reflections collected/unique/$[R_{int}]$	7241/7241/$[R_{int}]$ = 0.0522	7217/7217/$[R_{int}]$ = 0.0462	35,555/4787/$[R_{int}]$ = 0.0293
completeness to θ (%)	98.2	97.2	98.9
absorption correction	semi-empirical	semi-empirical	semi-empirical
max. and min. transmis.	0.7461 and 0.2506	0.7461 and 0.3802	0.7461 and 0.4860
refinement method	full matrix least-squares on $|F|^2$	full matrix least-squares on $|F|^2$	full matrix least-squares on $|F|^2$
data/restrains/parameters	7241/3/313	7217/0/298	4787/25/90
goodness of fit (GOF) on $|F|^2$	1.059	1.104	1.132
final R indices $[I > 2\sigma(I)]$	$R_1 = 0.0223$, $wR_2 = 0.0540$	$R_1 = 0.0389$, $wR_2 = 0.0986$	$R_1 = 0.0419$, $wR_2 = 0.0983$
R indices (all data)	$R_1 = 0.0241$, $wR_2 = 0.0547$	$R_1 = 0.0398$, $wR_2 = 0.0992$	$R_1 = 0.0487$, $wR_2 = 0.1032$
extinction coefficient	n/a	n/a	n/a
largest diff. peak and hole (e Å^{-3})	1.602 and −2.548	1.600 and −2.138	2.617 and −1.774

for some transition metal oxides, the D2 correction leads to cell parameters that are closer to experimental data than D3.[52,53] Ionic cores were described with projector-augmented wave pseudopotentials,[54,55] and the valence electrons were represented through a plane wave basis set with a kinetic energy cutoff of 400 eV. A (4,4,4) Monkhorst−Pack K-point mesh[56] was employed to describe the Brillouin zone. The energy convergence criteria were fixed to 10^{-5} and 10^{-4} eV for electronic and geometry relaxations, respectively. Further details about crystal structure refinement and electronic calculations are in the Supporting Information.

■ ASSOCIATED CONTENT

Ⓢ Supporting Information

The Supporting Information is available free of charge at https://pubs.acs.org/doi/10.1021/acsomega.0c04175.

Crystallographic data of compound **1** (CIF)
Crystallographic data of compound **2** (CIF)
Crystallographic data of compound **3** (CIF)
Crystallographic data of compound **4** (CIF)
Crystallographic data of compound **5** (CIF)
Crystallographic data of compound **6** (CIF)
Further details about crystal structures refinement, electronic calculations, PXRD, FTIR-ATR and ^{1}H NMR spectra, and TG/DTA determination (PDF)

Accession Codes

CCDC 2012988-2012993 contain the supplementary crystallographic data for this paper. These data can be obtained free of charge via www.ccdc.cam.ac.uk/data_request/cif, by emailing data_request@ccdc.cam.ac.uk, or by contacting The Cambridge Crystallographic Data Centre, 12 Union Road, Cambridge CB2 1EZ, UK; fax: +44 1223 336033.

■ AUTHOR INFORMATION

Corresponding Author

Josefina Pons − *Departament de Química, Universitat Autònoma de Barcelona, Barcelona 08193, Spain;* ⓞ orcid.org/0000-0002-9546-6828; Email: Josefina.Pons@uab.es

Authors

Francisco Sánchez-Férez − *Departament de Química, Universitat Autònoma de Barcelona, Barcelona 08193, Spain*
Xavier Solans-Monfort − *Departament de Química, Universitat Autònoma de Barcelona, Barcelona 08193, Spain*
Teresa Calvet − *Departament de Mineralogia, Petrologia i Geologia Aplicada, Universitat de Barcelona, Barcelona 08028, Spain*
Mercè Font-Bardia − *Unitat de Difracció de Raig-X, Centres Científics i Tecnològics de la Universitat de Barcelona (CCiTUB), Universitat de Barcelona, Barcelona 08028, Spain*

Complete contact information is available at:
https://pubs.acs.org/10.1021/acsomega.0c04175

Notes
The authors declare no competing financial interest.

■ REFERENCES

(1) Zarick, H. F.; Soetan, N.; Erwin, W. R.; Bardhan, R. Mixed Halide Hybrid Perovskites: A Paradigm Shift in Photovoltaics. *J. Mater. Chem. A* **2018**, *6*, 5507−5537.

(2) Oswald, I. W. H.; Ahn, H.; Neilson, J. R. Influence of Organic Cation Planarity on Structural Templating in Hybrid Metal-Halides. *Dalton Trans.* **2019**, *48*, 16340−16349.

(3) Chatterjee, S.; Pal, A. J. Influence of Metal Substitution on Hybrid Halide Perovskites: Towards Lead-Free Perovskite Solar Cells. *J. Mater. Chem. A* **2018**, *6*, 3793−3823.

(4) Berryman, O. B.; Bryantsev, V. S.; Stay, D. P.; Johnson, D. W.; Hay, B. P. Structural Criteria for the Design of Anion Receptors: The Interaction of Halides with Electron-Deficient Arenes. *J. Am. Chem. Soc.* **2007**, *129*, 48−58.

(5) Albrecht, M.; Wessel, C.; De Groot, M.; Rissanen, K.; Lüchow, A. Structural Versatility of Anion-π Interactions in Halide Salts with Pentafluorophenyl Substituted Cations. *J. Am. Chem. Soc.* **2008**, *130*, 4600−4601.

(6) Lim, J. Y. C.; Beer, P. D. Sigma-Hole Interactions in Anion Recognition. *Chem* **2018**, *4*, 731−783.

(7) Politzer, P.; Murray, J. S.; Clark, T.; Resnati, G. The σ-Hole Revisited. *Phys. Chem. Chem. Phys.* **2017**, *19*, 32166−32178.

(8) Nepal, B.; Scheiner, S. NX···Y Halogen Bonds. Comparison with NH···Y H-Bonds and CX···Y Halogen Bonds. *Phys. Chem Chem. Phys.* **2016**, *18*, 18015−18023.

(9) Melandri, S. "Union Is Strength": How Weak Hydrogen Bonds Become Stronger. *Phys. Chem. Chem. Phys.* **2011**, *13*, 13901−13911.

(10) Oswald, I. W. H.; Mozur, E. M.; Moseley, I. P.; Ahn, H.; Neilson, J. R. Hybrid Charge-Transfer Semiconductors: $(C_7H_7)SbI_4$, $(C_7H_7)BiI_4$, and Their Halide Congeners. *Inorg. Chem.* **2019**, *58*, 5818−5826.

(11) Savory, C. N.; Palgrave, R. G.; Bronstein, H.; Scanlon, D. O. Spatial Electron-Hole Separation in a One Dimensional Hybrid Organic-Inorganic Lead Iodide. *Sci. Rep.* **2016**, *6*, 20626−20627.

(12) Chen, W. T.; Zeng, X. R.; Fang, X. N.; Li, X. F.; Liu, L. M. Synthesis, Structure and Properties of $(4,4′-H_2Bipy)[HgBr_4] \cdot H_2O$ with Strong Fluorescence. *Inorg. Chem. Commun.* **2007**, *10*, 223−225.

(13) Smith, I. C.; Hoke, E. T.; Solis-Ibarra, D.; McGehee, M. D.; Karunadasa, H. I. A Layered Hybrid Perovskite Solar-Cell Absorber with Enhanced Moisture Stability. *Angew. Chem.* **2014**, *53*, 11232−11235.

(14) Mao, L.; Stoumpos, C. C.; Kanatzidis, M. G. Two-Dimensional Hybrid Halide Perovskites: Principles and Promises. *J. Am. Chem. Soc.* **2019**, *141*, 1171−1190.

(15) Cheng, P.; Wang, P.; Xu, Z.; Jia, X.; Wei, Q.; Yuan, N.; Ding, J.; Li, R.; Zhao, G.; Cheng, Y.; Zhao, K.; Liu, S. F. Ligand-Size Related Dimensionality Control in Metal Halide Perovskites. *ACS Energy Lett.* **2019**, *4*, 1830−1838.

(16) Albero, J.; Asiri, A. M.; García, H. Influence of the Composition of Hybrid Perovskites on Their Performance in Solar Cells. *J. Mater. Chem. A* **2016**, *4*, 4353−4364.

(17) Saparov, B.; Mitzi, D. B. Organic-Inorganic Perovskites: Structural Versatility for Functional Materials Design. *Chem. Rev.* **2016**, *116*, 4558−4596.

(18) Bharara, M. S.; Bui, T. H.; Parkin, S.; Atwood, D. A. Structure-Directing Influence of Halide in Mercury Thiolate Clusters. *Inorg. Chem.* **2005**, *44*, 5753−5760.

(19) Bharara, M. S.; Bui, T. H.; Parkin, S.; Atwood, D. A. Mercurophilic Interaction in Novel Polynuclear Hg(II)-2- Amino-ethanethiolates. *Dalton Trans.* **2005**, 3874−3880.

(20) Bharara, M. S.; Parkin, S.; Atwood, D. A. Solution and Solid-State Study of Heteroleptic Hg(II)-Thiolates: Crystal Structures of $[Hg_4I_4(SCH_2CH_2NH_2)_4]$ and $[Hg_4I_8(SCH_2CH_2NH_3)_2]$. *Inorg. Chem.* **2006**, *45*, 2112−2118.

(21) Bharara, M. S.; Parkin, S.; Atwood, D. A. Mercury(II) 2-Aminoethanethiolate Clusters: Intramolecular Transformations and Mechanisms. *Inorg. Chem.* **2006**, *45*, 7261−7268.

(22) Spengler, R.; Zouari, R.; Zimmermann, H.; Ben Salah, A.; Burzlaff, H. 1,3-Propanediammonium Tetrachloromercurate. *Acta Crystallogr. Sect. C Cryst. Struct. Commun.* **1998**, *54*, 1628−1631.

(23) Amami, M.; Zouari, R.; Ben Salah, A.; Burzlaff, H. 1,4-Butanediammonium Tetrachloromercurate(II). *Acta Crystallogr., Sect. E* **2002**, *58*, m357−m359.

(24) Belhouchet, M.; Wamani, W.; Mhiri, T. Synthesis, Structure and Spectroscopic Investigations of Two New Organic-Inorganic Hybrids $NH_3(C_6H_4)_2NH_3CuCl_4$ and $NH_3(C_6H_4)_2NH_3HgCl$. *IOP Conf. Ser.: Mater. Sci. Eng.* **2010**, *13*, No. 012039.

(25) Barbieri, A.; Accorsi, G.; Armaroli, N. Luminescent Complexes beyond the Platinum Group: The d^{10} Avenue. *Chem. Commun.* **2008**, 2185−2193.

(26) Guerrero, M.; Vázquez, S.; Ayllón, J. A.; Calvet, T.; Font-Bardia, M.; Pons, J. Zn(II) and Cd(II) Coordination Dimers Based on Mixed Benzodioxole-Carboxylate and N-Donor Ligands: Synthesis, Characterization, Crystal Structures and Photoluminescence Properties. *ChemistrySelect* **2017**, *2*, 632−639.

(27) Ejarque, D.; Sánchez-Férez, F.; Ayllón, J. A.; Calvet, T.; Font-Bardia, M.; Pons, J. Diverse Structures and Dimensionalities in Zn(II), Cd(II), and Hg(II) Metal Complexes with Piperonylic Acid. *Cryst. Growth Des.* **2020**, *20*, 383−400.

(28) Moreno-Gómez, L.; Sánchez-Férez, F.; Calvet, T.; Font-Bardia, M.; Pons, J. Zn(II) and Cd(II) Monomer, Dimer and Polymer Compounds Coordinated by Benzoic Acid and 4-Acetylpyridine: Synthesis and Crystal Structures. *Inorg. Chim. Acta* **2020**, *506*, 119561.

(29) Ali, B. F.; Al-Far, R. Isostructural Series of (2,2′-Bipyridinium) Tetrabromometallate(II); Intermolecular Interactions in the Structures of $(BpyH_2)[MBr_4]$; M = Zn Hg and Co. *J. Chem. Crystallogr.* **2008**, *38*, 689−693.

(30) Tsuge, M.; Lai, C. P.; Lee, Y. P. Infrared Spectra of 3-Hydroxy-(1H)-Pyridinium Cation and 3-Hydroxy-(1H)-Pyridinyl Radical Isolated in Solid Para -Hydrogen. *J. Chem. Phys.* **2018**, *149*, No. 014306.

(31) Rutkowski, K. S.; Melikova, S. M.; Rospenk, M.; Koll, A. Strong and Weak Effects Caused by Non Covalent Interactions between Chloroform and Selected Electron Donor Molecules. *Phys. Chem. Chem. Phys.* **2011**, *13*, 14223−14234.

(32) Golec, B.; Das, P.; Bahou, M.; Lee, Y.-P. Infrared Spectra of the 1-Pyridinium($C_5H_5NH^+$) Cation and Pyridinyl(C_5H_5NH and 4-C_5H_6N) Radicals Isolated in Solid Para-Hydrogen. *J. Phys. Chem. A* **2013**, *117*, 13680−13690.

(33) Williams, D. H.; Fleming, I. *Spectroscopic Methods in Organic Chemistry*; 7th ed.; Springer Nature: Cham, Switzerland, 2008.

(34) Teleb, S. M.; Gaballa, A. S. Preparation and Spectroscopic Studies on Charge-Transfer Complexes of 2,2′-Bipyridine with Picric and Chloranilic Acids. *Spectrochim. Acta, Part A* **2005**, *62*, 140−145.

(35) Yang, L.; Powell, D. R.; Houser, R. P. Structural Variation in Copper(I) Complexes with Pyridylmethylamide Ligands: Structural

Analysis with a New Four-Coordinate Geometry Index, T4. *J. Chem. Soc Dalton Trans.* **2007**, *9*, 955−964.

(36) Rabeand, S.; Müller, U. Crystal Structure of Bis-(Tetraphenylphosphonium) Octachlorotrimercurate, [P-(C$_6$H$_5$)$_4$]$_2$[Hg$_3$Cl$_8$]. *Zeitschrift für Krist. - New Cryst. Struct.* **1999**, *214*, 277−278.

(37) Fernando, I. R.; Mezei, G. Blue-Colored, Linear Rigid-Axle [2]Pseudorotaxanes: Metal-Binding Properties, Crystal Structures, and Blue/Red Dichroism. *Inorg. Chem.* **2012**, *51*, 3156−3160.

(38) Xu, L.; Gao, J. X.; Chen, X. G.; Hua, X. N.; Wu, D. H.; Liao, W. Q. Unprecedented Dielectric Bistable Switching in a Binuclear Hg(II) Based Hybrid Compound. *Eur. J. Inorg. Chem.* **2019**, *2019*, 800−807.

(39) Oueslati, A.; Chaabane, I.; Adil, K.; Hlel, F. Structural Characterization and Infrared and Electrical Properties of the New Inorganic-Organic Hybrid Compound [N(C$_3$H$_7$)$_4$]$_2$[Hg$_2$Cl$_6$]. *J. Chem.* **2013**, *2013*, 1−10.

(40) Chen, J.-X.; Zhang, W.-H.; Ren, Z.-G.; Zhang, Y.; Lang, J.-P. Bis[4(Trimethylammonio)Phenyl]Disulfide Tetraiodomercurate(II). *Acta Crystallogr., Sect. E: Struct. Rep. Online* **2005**, *61*, 60−62.

(41) Ishihara, H.; Horiuchi, K.; Svoboda, I.; Fuess, H.; Gesing, T. M.; Buhl, J.-C.; Terao, H. Crystal Structures of Piperazinium Tetrahalogenometallates (II)[C$_4$H$_{12}$N$_2$]MX$_4$ (M = Zn, Hg; X = Br, I). *Z. Naturforsch. B* **2006**, *61*, 69−72.

(42) Ye, Z. Y.; Zhang, Z. Y.; Huo, L. H.; Deng, Z. P.; Zhang, X. F.; Gao, S. Mercury Supramolecular Architectures Constructed from Flexible Unsymmetrical Bis(Pyridyl) Ligands: Structural Motif Mediated by Mercury-Halide Clusters, Ligand Conformations and Non-Covalent Interactions. *Polyhedron* **2016**, *117*, 338−351.

(43) Govindan, E.; Thirumurugan, S.; Ganeshraja, A. S.; Anbalagan, K.; Subbiahpandi, A. Bis(1,10-Phenanthrolin-1-Ium) Tetrachlorido-zincate Monohydrate. *Acta Crystallogr., Sect. E* **2014**, *70*, m53.

(44) Feng, G.; Evangelisti, L.; Favero, L. B.; Grabow, J. U.; Xia, Z.; Caminati, W. On the Weak O-H···halogen Hydrogen Bond: A Rotational Study of CH$_3$CHClF···H$_2$O. *Phys. Chem. Chem. Phys.* **2011**, *13*, 14092−14096.

(45) Turner, M. J.; McKinnon, J. J.; Wolff, S. K.; Grimwood, D. J.; Spackman, P. R.; Jayatilaka, D.; Spackman, M. A. CrystalExplorer17. *University of Western Australia*, 2017.

(46) Hernández-Haro, N.; Ortega-Castro, J.; Martynov, Y. B.; Nazmitdinov, R. G.; Frontera, A. DFT Prediction of Band Gap in Organic-Inorganic Metal Halide Perovskites: An Exchange-Correlation Functional Benchmark Study. *Chem. Phys.* **2019**, *516*, 225−231.

(47) Göller, A.; Grummt, U. W. Torsional Barriers in Biphenyl, 2,2′-Bipyridine and 2-Phenylpyridine. *Chem. Phys. Lett.* **2000**, *321*, 399−405.

(48) Perdew, J. P.; Burke, K.; Ernzerhof, M. Generalized Gradient Approximation Made Simple. *Phys. Rev. Lett.* **1996**, *77*, 3865−3868.

(49) Grimme, S. Accurate Description of Van Der Waals Complexes by Density Functional Theory Including Empirical Corrections. *J. Comput. Chem.* **2004**, *25*, 1463−1473.

(50) Kresse, G.; Hafner, J. Ab Initio Molecular Dynamics for Liquid Metals. *Phys. Rev. B* **1993**, *47*, 558−561.

(51) Kresse, G.; Furthmüller, J. Efficient Iterative Schemes for Ab Initio Total-Energy Calculations Using a Plane-Wave Basis Set. *Phys. Rev. B* **1996**, *54*, 11169−11186.

(52) Heras-Domingo, J.; Sodupe, M.; Solans-Monfort, X. Interaction between Ruthenium Oxide Surfaces and Water Molecules. Effect of Surface Morphology and Water Coverage. *J. Phys Chem. C* **2019**, *123*, 7786−7798.

(53) González, D.; Heras-Domingo, J.; Pantaleone, S.; Rimola, A.; Rodríguez-Santiago, L.; Solans-Monfort, X.; Sodupe, M. Water Adsorption on MO$_2$ (M = Ti, Ru, and Ir) Surfaces. Importance of Octahedral Distortion and Cooperative Effects. *ACS Omega* **2019**, *4*, 2989−2999.

(54) Blöchl, P. E. Projector Augmented-Wave Method. *Phys. Rev. B* **1994**, *50*, 17953−17979.

(55) Kresse, G.; Joubert, D. From Ultrasoft Pseudopotentials to the Projector Augmented-Wave Method. *Phys. Rev. B - Condens. Matter Mater. Phys.* **1999**, *59*, 1758−1775.

(56) Pack, J. D.; Monkhorst, H. J. "special Points for Brillouin-Zone Integrations"-a Reply. *Phys. Rev. B* **1977**, *16*, 1748−1749.